

Enhanced Long Wavelength Mermin-Wagner Fluctuations in Two-Dimensional Active Crystals and Glasses

Subhodeep Dey,¹ Antik Bhattacharya,¹ and Smarajit Karmakar^{1,*}

¹*Tata Institute of Fundamental Research Hyderabad,
36/P, Gopanpally Village, Serilingampally Mandal,
Ranga Reddy District, Hyderabad, Telangana 500046, India*

In the realm of two-dimensional (2D) systems, the renowned Mermin-Wagner effect plays a significant role, giving rise to striking dimensionality effects marked by far-reaching density fluctuations and the divergence of various dynamic properties. This effect also unequivocally negates the possibility of stable crystalline phases in 2D particulate systems characterized by continuous degrees of freedom. This effect has been recently discerned in glass-forming liquids, displaying characteristic signatures like the logarithmic divergence of mean squared displacement in the plateau regime. We explored these long-wavelength fluctuations in crystalline solids and in glass-forming liquids in the presence of non-equilibrium active forces. These systems are known in the literature as active crystals and glasses, and they can be thought of as a minimalistic model for understanding various non-equilibrium systems where the constituent particles' dynamics are controlled by both temperature and other active forces, which can be external or internal. Such models often offer valuable insights into the dynamical behavior of biological systems, such as collections of cells, bacteria, ant colonies, or even synthetic self-propelled particles like Janus colloids. Our study reveals that fluctuations stemming from active forces get strongly coupled with long wavelength fluctuations arising from thermal effects, resulting in dramatic dynamical effects, particularly in 2D systems. We also shed light on how these fluctuations impact dynamical heterogeneity, a defining characteristic of glassy dynamics.

I. INTRODUCTION

The arguments of Mermin-Wagner [1, 2] on the absence of true long-range crystalline order in 2D systems with continuous degrees of freedom highlight the effect of long-wavelength modes of density fluctuations on both the structure and the dynamics of the system. According to the well-known KTHNY (Kosterlitz-Thouless-Halperin-Nelson-Young) theory [3–5] due to the presence of topological defects, a perfect crystal in 2D does not exist. It is often argued in the theoretical derivation of the Mermin-Wagner (MW) theorem that the dispersion behaviour of phonons determines the thermal vibrations of the molecules or particles in their equilibrium crystalline position, and it is quite straightforward to show that the mean squared displacement (MSD) of particles from their equilibrium position, also known as the Debye-Waller (DW) Factor, diverges logarithmically with the linear size (L) of the system in 2D and even strongly in one-dimension (1D).

The Mermin-Wagner theorem states that the stability of a solid is influenced by phonons. It does not require crystalline order to hold true and applies as long as phonon-like excitations exist in the system at a large enough length scale, Mermin-Wagner arguments will always lead to logarithmic divergence of the MSD of the particles. Recent studies [6] have shown that long wavelength density fluctuations affect not only the solid states of matter but also dynamics in the liquid states in 2D systems. This is why such effects can also be observed in

supercooled liquids and amorphous solids [7]. The difference in dynamical behavior between 2D and 3D systems can be explained by the presence of long wavelength fluctuation. For 2D colloidal systems, the presence of such fluctuations has been confirmed by recent works[8–10]. Furthermore, recent studies [6] have shown that MW fluctuations have significantly strong effects even at high temperatures that are way higher than the supercooled temperature regimes. At these high temperatures, the Stokes-Einstein relation breaks down due to the decoupling of relaxation time and diffusivity, which is different from the breakdown observed in supercooled temperature regimes.

Stokes-Einstein (SE) relation is a dynamical relation between the diffusivity (D) of the particles in the medium and the characteristic relaxation time (τ_α) or viscosity (η) as

$$D \propto \frac{K_B T}{C \eta} = \frac{1}{C' \tau_\alpha}, \quad (1)$$

with K_B being the Boltzmann constant, C and C' being a constant that depends on the details of the particles or probe under consideration. The last equation is obtained using the approximation that $\tau_\alpha \simeq \eta/K_B T$, which has been validated in previous works [11]. In the supercooled temperature regime, one often finds the following equation to be obeyed: $D \propto \tau_\alpha^{-\kappa}$, with κ being smaller than 1. This has been validated in various glass-forming liquids in experiments and simulations of model glass-forming systems in 3D and has been convincingly established that the observation can be explained using the concept of dynamic heterogeneity in these systems and

* smarajit@tifrh.res.in

an associated correlation length[12]. Whereas in 2D systems, the picture is very different at high temperatures. $\kappa > 1$ is reported in the high-temperature normal liquid regimes of 2D glass-forming liquids whereas $\kappa < 1$ being reported in the supercooled temperature regime similar to the 3D case. The observation of $\kappa > 1$ at normal liquids in 2D has been convincingly demonstrated as purely coming from the Mermin-Wagner-like long-wavelength density fluctuations in the system, thereby proving that Mermin-Wagner fluctuations are prevalent even at high temperatures as much as in supercooled and solid temperature regimes[6].

A hallmark characteristic of glassy dynamics is the enhanced dynamical heterogeneity, which quantifies the marked difference in relaxation patterns in different parts of a glassy system [13–15]. Dynamic heterogeneity is often highlighted as one of the important features of glassy dynamics. In a recent work [16], it has been demonstrated via measurement of four-point dynamic susceptibility ($\chi_4(t)$, defined in the Methods section) that long wavelength phonon gets coupled if one introduces additional driving in the system at the particle level say via active driving. In such a scenario, $\chi_4(t)$ develops an additional short-time peak, which grows with increasing strength of the driving or the activity. It was also found that the short-time peak of $\chi_4(t)$ increases with increasing system sizes, and the peak position linearly increases with L . Additionally, the short time peak of $\chi_4(t)$ disappears if one does Brownian dynamics simulation of the same systems in the over-damped limit where the phonons get suppressed considerably, thereby significantly reducing the effect of phonons in the dynamics. These results suggest that non-thermal active driving plays a prominent role in the short-time dynamics, especially by enhancing the phonon-like excitations in the systems. Naturally, the question that arises is the following. If one studies active glass-forming liquids in 2D, would the Mermin-Wagner long wavelength excitations get even more enhanced, leading to a stronger divergence of the Debye-Waller factor? The study of active particulate systems in 2D is of interest primarily because of various experimental situations where 2D or quasi-2D geometry is often adopted for experimental feasibility. Various biological systems, including mono-layer of tissues, which show glass-like dynamics, can be considered quasi-2D systems. In this work, we have performed extensive computational studies on the dynamics of 2D crystalline and polycrystalline solids along with two model 2D active glasses [16], especially to understand how active forces get coupled with the long wavelength phonon excitations and their possible implications on various dynamical observables, including dynamical heterogeneity

In recent times, there has been a surge of research activities in the field of active matter, leading to the emergence of a new direction of studies on disordered systems called active glasses [12, 17]. Active matter is often categorized as a system in which the constituents can move internally, driven by their internal energy, in addition

to the environmental influence of thermal fluctuations [18–22]. Such systems exhibit a plethora of interesting dynamical phenomena, including spontaneous symmetry breaking of the rotational order in two dimensions [18] leading to the formation of ordered phases of clusters or flocks. These clusters have coherent collective motion at low noise strength and high particle density [19]. Many biological systems exhibit collective dynamical behavior, in which forces generated by ATP consumption drive the dynamics instead of thermal fluctuations. A simple model of these systems that can capture some of the salient dynamical behaviors is a collection of self-propelled particles (SPPs) [22]. Several studies show that collective dynamics of cells and tissues during cell proliferation, cancerous cell progression, and wound healing [23–32] have dynamical features similar to glassy dynamics. Cell cytoplasm and bacterial cytoplasm show glassy dynamics, which can also modulate the depletion of ATP [23, 25]. These intricate dynamical similarities between various biological systems and glassy systems have fuelled a lot of research activities in modeling active glassy systems to develop an understanding of the emergent dynamical behaviors that are not very sensitive to the details of the system. Instead, they are outcomes of intrinsic non-equilibrium driving due to active forces [33].

Active systems are inherently out of equilibrium in nature as they do not follow detailed balance and are driven either internally or by external forcing. In recent years, there have been attempts to understand their steady-state dynamical behavior within equilibrium statistical mechanics using an appropriate effective temperature. Analytical results on the dynamics of an active particle in a harmonic potential, also known as active Ornstein-Uhlenbeck process, suggest that an effective temperature-like dynamics accurately describes the dynamical process of the active particle [33]. Similar ideas have been extended to active glasses, which suggest that some dynamical aspects can be well understood using an effective temperature description [17, 34–39]. However, higher-order dynamical correlation functions like four-point susceptibility ($\chi_4(t)$) cannot be understood with the same effective temperature description, as reported in [12]. Thus, a clear understanding of active systems in their dynamical steady states is still lacking, and the intricate effects of active driving on the dynamics continue to puzzle the scientific community.

In this article, we explore the impact of activity on the dynamics of polycrystalline solids, in addition to two 2d glass-forming model systems. These models, referred to as 2dmKA and 2dKA, are characterized by varying degrees of local structural ordering. The former is a generic model of glass-forming liquids, while the latter exhibits growing local or medium-range crystalline order (MRCO) as temperature decreases. Our simulations are carried out in the NVT ensemble, with system sizes ranging from $N = 100$ to 10^5 particles. To introduce activity into the system, we use run and tumble particle (RTP) dynamics [16, 17, 40], which can be tuned using three parameters:

c , f_0 , and τ_p . The concentration of active particles, c , is varied in the range $c \in [0, 0.6]$, while the strength of the active force applied to each particle, f_0 , is varied in the range $f_0 \in [0, 2.5]$. The persistent timescale, τ_p , determines the duration for which the active forces act along a fixed but random direction, and is varied in the range $\tau_p \in [0, 100]$ in our simulations. Additionally, we have performed Brownian dynamics simulations of these models to compare and contrast their behavior with that of the active systems. Further details of the models and simulation protocols are provided in the Method section.

Our study shows that the Mermin-Wagner effect is prominent even at higher temperatures, consistent with the findings in passive systems. We have also demonstrated the impact of phonon-like excitations in these systems by calculating an effective dynamical matrix. Our results have shown that the mechanisms of Mermin-Wagner physics still hold in non-equilibrium systems, but with greater strength. We have observed that the Debye-Waller factor diverges as a power-law with increasing activity strength, instead of the usual logarithmic divergence seen in equilibrium systems. Interestingly, we have also found that the phonon dispersion relation gets modified to a non-linear dependence on wave vector with increasing activity. Furthermore, we have discovered that the first peak of $\chi_4(t)$, directly linked to the system's underlying phonon, grows rapidly with increasing system size and activity. We have identified a unique feature of the effect of activity in two different model glass-formers; specifically, we have observed that in the 2dmKA model, the long-time peak of $\chi_4(t)$ decreases with increasing activity, along with a decrease in the characteristic timescale. In contrast, for the 2dKA model, we have seen that the peak height of $\chi_4(t)$ increases with increasing activity, although the characteristic timescale decreases. Our findings shed light on the surprising and unique feature of systems with local or medium-range crystalline order (MRCO). This may explain the recent experiments on cellular monolayers, where it was discovered that dynamic heterogeneity (DH) increases with increasing activity in the medium, while the relaxation time decreases systematically.

II. RESULTS

Dynamical Measurements: To explore the enhanced effect of long wavelength phonon modes in active crystals and glasses, we first computed the mean squared displacement (MSD), $\langle \Delta r^2(t) \rangle$, as a function of time for 2dmKA model glass-forming liquids with a strength of activity of $f_0 = 2.0$ at a reduced temperature of $T = 0.221$. We used system sizes of $N = 10^3, 10^4$, and 10^5 , and the results are presented in Fig.1(A). The definition of MSD can be found in the Methods section. The inset of the same panel shows the data for passive systems. We observed a significant increase in the plateau value of MSD for active systems compared to the pas-

sive scenario at similar relaxation times, demonstrating the enhanced effect of long wavelength fluctuations due to active forcing. In Fig.1(B), we explored the decay profile of the two-point density correlation function $Q(t)$ for the same system sizes as in panel A. This was done to demonstrate how long wavelength fluctuations lead to faster relaxation in active systems for larger system sizes. The inset shows the relaxation profile for passive systems. Next, we computed the plateau value of MSD for varying system sizes and activity strength f_0 , while keeping the concentration of active particles ($c = 0.1$) and persistent time ($\tau_p = 1.0$) fixed. The results are presented in Fig.1(C). We defined the plateau value of MSD as $MSD(\tau)$ with τ being the time at the plateau. We observed a faster than logarithmic, in fact, a power law divergence, $MSD(p) \sim L^\delta$, in the presence of active particles, while there was a $\log(L)$ type divergence of $MSD(\tau)$ for passive systems. The exponent δ seems to be increasing systematically with increasing activity strength f_0 with $\delta \sim 0.9$ for $f_0 = 2.0$. We obtained similar results when varying c while keeping f_0 constant. Thus, the results appear to be independent of the particle choice of the activity parameter.

Observing the strong effect of long wavelength fluctuations in disordered systems, led us to investigate their effect on active crystalline and polycrystalline solids. Our findings, presented in Fig. 1(D), show that the plateau value of the mean squared displacement (MSD) significantly increases with system size in the presence of activity ($f_0 = 2.0$), while for passive systems, the growth of MSD plateau follows a logarithmic divergence (see inset). We also plotted the MSD plateau values as a function of system size in a double logarithmic plot, presented in Panel E of the same figure, which shows that the divergence of MSD plateau or the Debye-Waller factor in active crystals grows as power-law in system size, similar to the results found in disordered systems. The exponent $\delta \sim 1.65$ seems to be stronger than the exponent obtained in disordered solids. These observations suggest that structural ordering does not play a role in these dynamic phenomena, as is the case for Mermin-Wagner fluctuations.

To see whether the long wavelength fluctuations affect the dynamics of active liquids at high enough temperatures where the effect of active force is much weaker than the thermal fluctuations, we have plotted the diffusivity (D) as a function of characteristic relaxation time, τ_α following Eqn.1. The relaxation time (τ_α) can be computed using $\langle Q(t = \tau_\alpha) \rangle = 1/e$ and D is computed from the slope of MSD vs t at long timescale. Indeed, D vs τ_α plot shows a power-law relation with exponent (κ) larger than 1 ($\kappa \simeq 1.35$) at high temperatures and then at supercooled temperature regime $\kappa \simeq 0.80$ indicating the validity of well-known fractional Stokes-Einstein relation. The violation of SE relation at high temperature with $\kappa > 1.0$ again corroborates with the previous observation of the effect of long wavelength phonon fluctuations in 2D passive liquids. Thus, a phonon-like effect

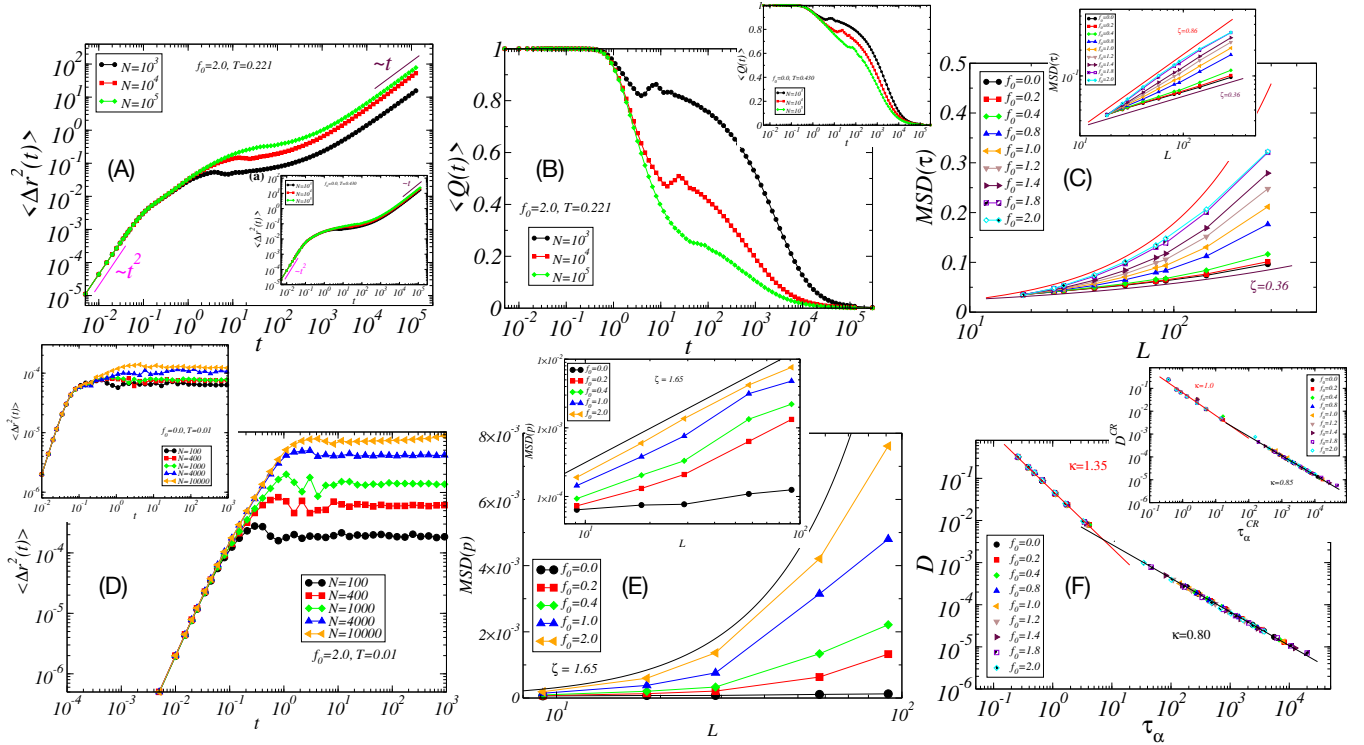


FIG. 1. (A) Mean square displacement (MSD) as a function of time for activity $f_0 = 2.0$ at temperature $T=0.221$ with system size ranging from 10^3 to 10^5 , here it shows increase in MSD plateau much faster than the passive system (Inset) at temperature $T=0.430$. This effect. (B) Two point density correlation $Q(t)$ shows faster relaxation for the case of active system than the passive system (Inset) for large system size. (C) $MSD(\tau)$ plateau diverges faster than $\log(L)$ increasing activity. Inset: At larger activity it starts to power-law behavior unlike $\log(L)$ behavior of its passive counter-part. For $f_0 = 2.0$ the power exponent is $\zeta = 0.86$. (A), (B) & (C) are for 2dmKA system. (D) MSD as function of time for active polycrystalline system for $f_0 = 2.0$ at temperature $T=0.01$ for system ranging from 10^2 to 10^4 , it shows faster increase in MSD plateau than passive system (Inset) at same temperature similar to (A). (E) For active polycrystal we can get similar power-law of MSD plateau divergence, here for activity $f_0 = 2.0$ the exponent is $\zeta = 1.65$. (F) Diffusivity as a function of relaxation time shows a power-law exponent $\kappa = 1.35$. this breakdown of Stokes-Einstein relation ($\kappa > 1.0$) is possible due to the presence of long wavelength phonon fluctuation in 2D, which is also valid for active system as well. We again get back the Stokes-Einstein relation with $\kappa \simeq 1.0$ when we do cage-relative diffusivity and relaxation time calculations, again showing the presence of phonon like excitations in active liquids as well.

persists even for active liquids, suggesting a possible effective phonon-like dynamical behaviour in these active liquids and solids. In the inset of the same figure panel, we plot D vs τ_α after removing the long wavelength fluctuations by computing cage-relative methods as detailed in the Methods section. One sees the validity of SE relation with $\kappa \simeq 1$ at high temperature reinforcing the phonon-like excitations in active liquids.

Effective Dynamical Matrix & Phonons: In order to investigate the phonon-like behavior of active liquids, crystals, and glasses at low temperatures, we employed a method to compute the effective dynamical matrix of the systems. This involved calculating the displacement-displacement covariance matrix, as explained in Refs. [41, 42]. The covariance matrix (C) is defined as $C_{ij}^{\alpha\beta} = \langle u_i^\alpha u_j^\beta \rangle$, where u_i represents the displacement of the i^{th} particle from its minimum position, and α or β represent the spatial dimensions (such as x or

y in 2D). The symbol $\langle \dots \rangle$ denotes ensemble and time averaging. While exploring different approaches to computing the dynamical matrix, we found that the force-force correlation matrix method did not work well for active systems that lack a Hamiltonian structure, where the forces cannot be derived from a potential. However, this method proved successful for passive systems. More information on this is available in the Supplementary Material (SM). Therefore, in this study, we focused on the results obtained using the displacement-displacement covariance matrix, which, although computationally expensive, provided a good description of the system at a coarse-grained timescale. To obtain better convergence, we computed the correlation matrix at a timescale as small as a few molecular dynamics (MD) steps up to the largest timescale accessible. This is important to get good convergence for all frequencies. We carried out the computations on energy-minimized structures for the dis-

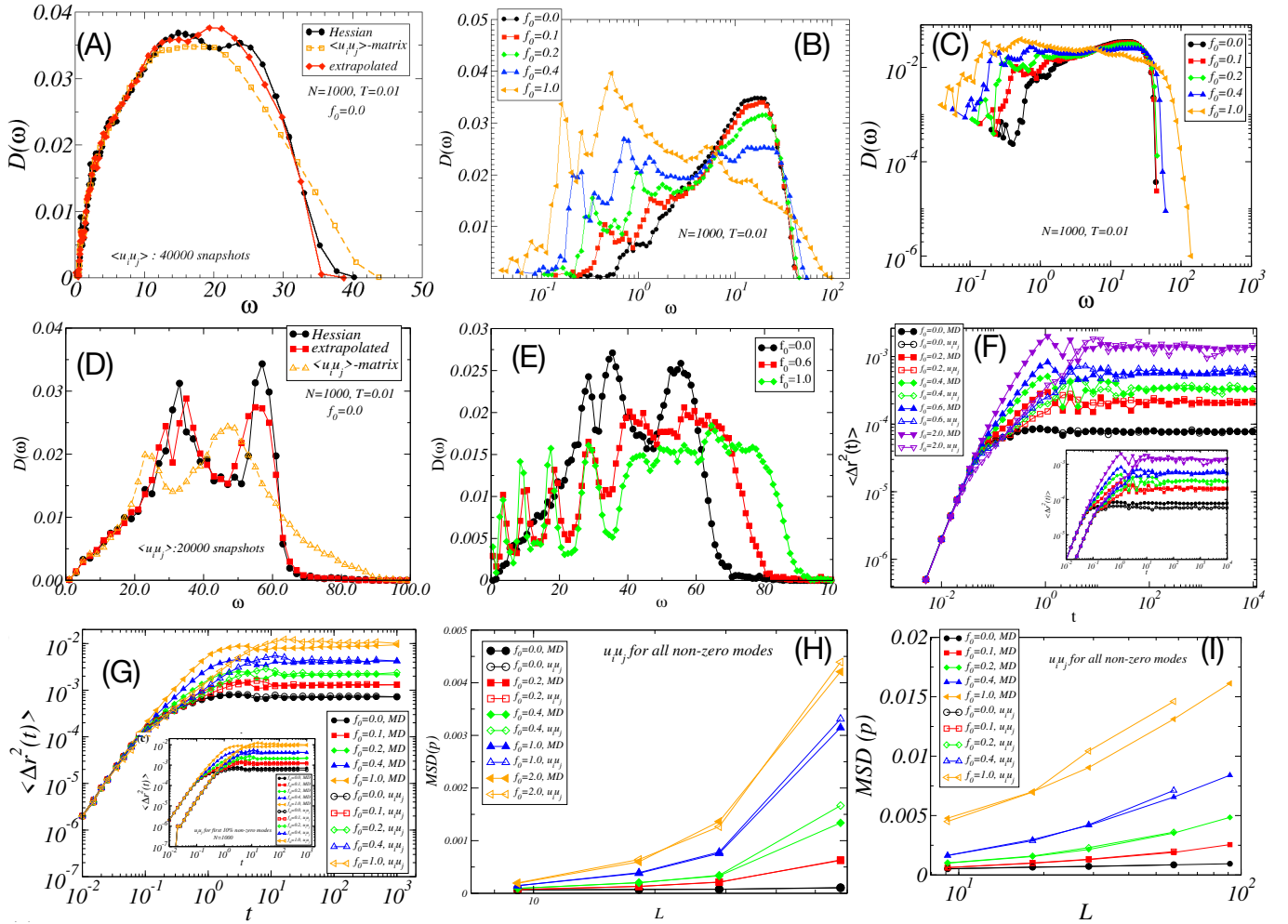


FIG. 2. **Effective Density of States (DoS) and Phonons:** (A) DoS computed for passive systems for $N = 1000$ particles using exact diagonalization of the Hessian matrix (black circle), averaged displacement-displacement correlation matrix (orange square) and corrected via random matrix procedure (red diamond) (see text for details). The close agreement between these measurements suggests that the displacement-displacement correlation matrix method with random matrix correction is a robust method for the computation of DoS. (B & C) DoS is computed using the displacement correlation matrix method for active systems with increasing activity. The clear appearance of small frequency (ω) peaks in the DoS with increasing activity signals the increasing dominance of phonon-like modes. The increasing weight of DoS at small ω also indicates a jamming to unjamming scenario. (D) & (E) DoS computed for passive and active polycrystalline samples, respectively. (F) The measured MSD was compared with computed MSD from the correlation matrix. The excellent agreement suggests the validity of the effective dynamical matrix description of these active systems even at a significant degree of activity. (G) shows the same comparison for amorphous solids. Inset (F) and (G) highlight the importance of small ω modes in determining the plateau value of the MSD for all activities. (H) and (I) Comparison of plateau values vs system size, L , as obtained from MD simulations and from effective dynamical matrix description. This proves that dramatic Mermin-Wagner (MW) fluctuations in the active matter are due to the phonons, and thus, deviation of MW theorem has to come from the details of the phonon dispersion relation. (F) & (H) is for polycrystalline system, and (G) & (I) is for amorphous solid.

ordered systems, polycrystalline, and crystalline solids we studied. This approach ensured that the matrix's eigenvalues were all positive, giving us an opportunity to validate the method's accuracy. Further details on this method can be found in the Method section and in the SM.

In Fig.2(A), we show the obtained density of state (DoS) obtained from the dynamical matrix \mathcal{C} averaged

over 64 independent ensembles. The DoS obtained from the Hessian matrix \mathcal{H} (see Methods for the definition) is labelled as "Hessian", and the one obtained using displacement-displacement correlation is labelled as " $\langle u_i u_j \rangle$ matrix". Within Harmonic approximation, one can show $\mathcal{C} = (1/T)\mathcal{H}^{-1}$, where T is the temperature at which the displacement correlation matrix is obtained. The matrix so obtained does not depend on the partic-

ular choice of temperature as long as the temperature is low enough that the Harmonic approximation is a faithful description of the system, and during the simulation timescale, it does not escape out of the minimum.

In panel A of the same figure, we present a corrected Density of States (DoS) referred to as "extrapolated". We corrected the DoS using a random matrix protocol, as described in detail in [41, 42] (see SM). In brief, we obtained the \mathcal{C} matrix and calculated the eigenvalues ($\lambda = \omega^2$) of the matrix via numerical diagonalization procedure at various degrees of increasing ensemble averaging. Then, we re-estimated these eigenvalues via extrapolation to the infinite ensemble averaging limit based on results on random matrix theory, which suggest that the eigenvalues reach their true limiting values linearly with increasing averaging. The corrected DoS matches well with the DoS computed from the Hessian matrix as shown in panel A. We then used this procedure to obtain the dynamical matrix for active systems with increasing activity, as shown in Fig.2(B). We observed that the DoS develops significant weight at smaller ω , along with sharp peaks resembling the prominence of phonon-like modes at lower frequencies. The peaks become sharper and stronger with increasing activity. We represented the DoS in a double logarithm plot in Fig.2(C) to highlight the similarity with the DoS for jammed states approaching the unjamming transition. While it is true that with increasing activity one approaches fluidization, the unjamming transition does not promote phonon-like excitations in the system. A detailed analysis is required to understand this similarity. In Fig.2(D), we show our results for polycrystals without activity, and panel (E) shows the same with increasing activity, echoing the similar observation of enhanced phonon excitations with increasing activity.

After reliable numerical computation of the DoS, we wanted to verify the validity of this effective dynamical matrix in describing the dynamics by computing the MSD from the obtained eigenvalues and eigenvectors of the dynamical matrix, \mathcal{C} as (see SM for the derivation)

$$\langle \Delta r(t)^2 \rangle = \frac{K_B T}{N} \left[\sum'_{a,i} (\vec{P}_i^a)^2 \frac{\sin^2(\omega_a t/2)}{(\omega_a/2)^2} \right], \quad (2)$$

where \vec{P}_i^a is the i^{th} component of the eigenvector a and ω_a is the corresponding eigenvalue. In Figs. 2(F) and 2(G), we compare the computed MSD from Eqn. 2 with the one obtained from the molecular dynamics (MD) simulation trajectories for polycrystal and amorphous solids, respectively. We observe a perfect match for the passive case, and a very good match for the active system. However, increasing activity strength shows a mismatch at intermediate timescales when the system transitions from the ballistic to the plateau regime. Despite this, both the short-time ballistic regime and the plateau regime are well-captured by the effective dynamical matrix. Although it is not immediately clear why there is a dis-

crepancy at the intermediate timescale when the system transitions from the ballistic to the plateau regime, we can postulate that with increasing strength of the active forcing, the system will take a longer time to lose its memory of active driving in the particle displacement. This means that particles will continue to move in the same direction of the applied force for a longer time, leaving the displacement correlated in a manner that cannot be described by an effective equilibrium-like description. However, at a longer timescale, the system will start to move towards the diffusive regime, and we believe that an effective dynamical matrix description will not be a poor description. Thus, we expect that if we take only a few of the low-frequency modes of \mathcal{C} and compute the MSD, we can correctly capture the plateau values for all activities. In the inset of Figs. 2(F) and 2(G), we show that the MSD computed using Eqn. 2 with only the first 10% of the low-frequency modes indeed correctly captures the plateau value for all activities. These results suggest that the long-time behavior of the active system confined in a potential minimum can be accurately described by an effective dynamical matrix.

Effective Phonon Dispersion: After establishing the effective phonon-like description of the active systems at low temperatures and thereby providing strong evidence of phonon being the main reason behind the observed enhancement of Mermin-Wagner fluctuations, we want to understand the primary cause for the breakdown of the MW theorem. Suppose we assume the basic mechanisms of MW arguments hold through. In that case, one expects that the phonon dispersion relation, which gives the dependence of ω on the wave vector q must get modified due to the presence of active forces as follows:

$$\langle \Delta x^2 \rangle \sim \int_{\frac{2\pi}{L}}^{\frac{2\pi}{\sigma}} \frac{q dq}{|\omega(q)|^2} \sim L^{2(\alpha-1)}, \quad (3)$$

where we have assumed $\omega(q) \sim q^\alpha$. In the limit $\alpha \rightarrow 1$, we get back the usual logarithmic dependence, but for $\alpha > 1$, we will have a power-law divergence of the MSD with increasing system size. Thus, a non-linear phonon-dispersion relation in active systems can rationalize the observation. Microscopic understanding of why one expects a non-linear phonon dispersion relation is now clear.

In Fig.3(A), we show the heat map of the ω vs q for longitudinal spectrum of the polycrystalline samples with activity $f_0 = 1.0$. In panel (B) shows the peak of heat map giving us the phonon dispersion relation of $\omega(q)$. The linear phonon dispersion relation for passive system is very clear and increasing non-linearity in active systems is also very evident, Inset: log-log plot of the same plot shows the power-law exponent of the dispersion relation. For activity $f_0 = 1.0$, $\alpha \sim 1.8$. In panel (C), we show the dispersion relation for the transverse spectrum of the polycrystalline samples, the exponent $\alpha \sim 1.74$. Panel (D) shows the heat map of the ω vs q for longitudinal spectrum of the amorphous solid $f_0 = 1.0$ and

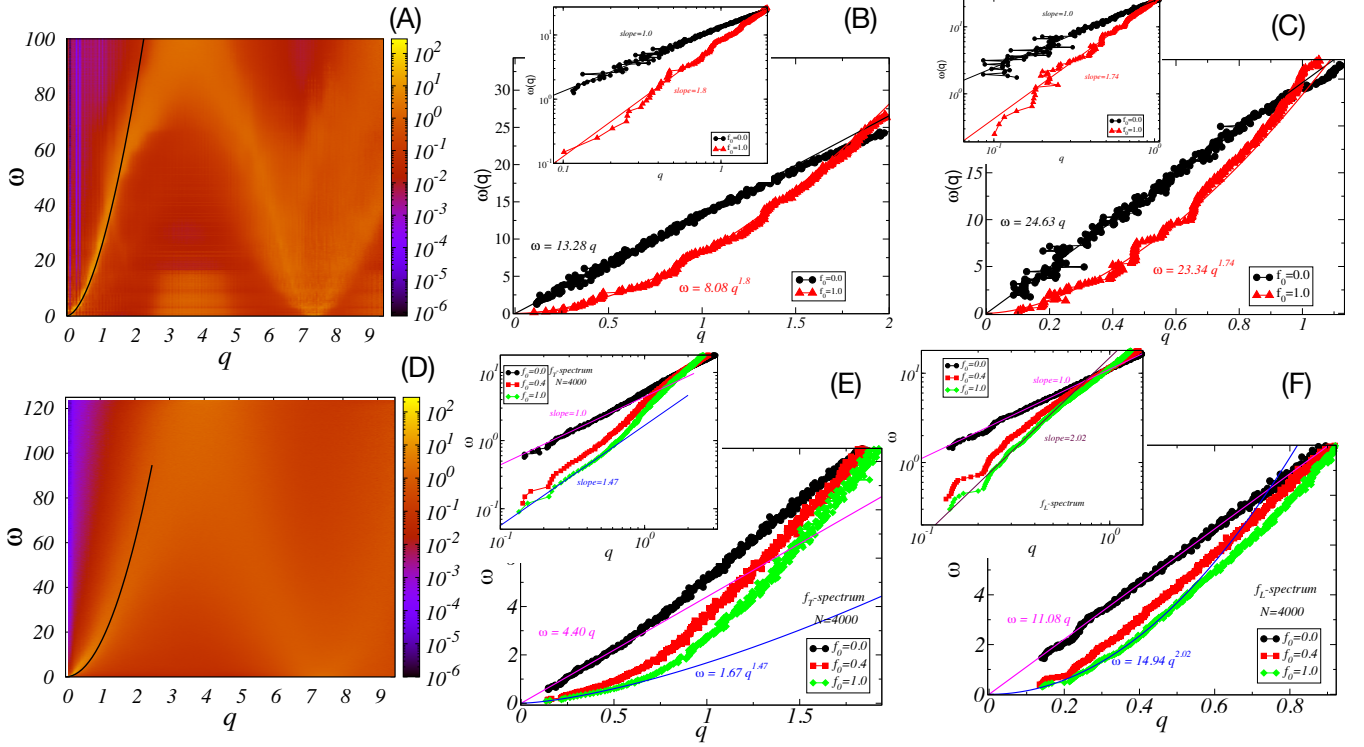


FIG. 3. **Effective phonon dispersion:**(A) Heat map of the ω vs q for longitudinal spectrum of the polycrystalline samples with activity $f_0 = 1.0$. (B) shows the peak of heat map giving us the phonon dispersion relation of $\omega(q)$. The linear phonon dispersion relation for passive system is very clear and increasing non-linearity in active systems is also very evident, where for activity $f_0 = 1.0$ exponent is $\alpha \simeq 1.8$. Inset: log-log plot of the same. (C) the transverse spectrum of the polycrystalline samples for activity $f_0 = 1.0$ shows the dispersion exponent $\alpha \simeq 1.74$. (D) we show the heat map of the ω vs q for longitudinal spectrum of the amorphous solid samples with activity $f=1.0$. (E) for amorphous solids samples with varying degree of activities. The spectrum is obtained for the longitudinal phonons and the inset shows the results in log-log plot. The exponent of the power law relation for activity $f_0 = 1.0$, $\alpha \simeq 1.47$. (F) shows the similar results but for transverse phonons with activity $f_0 = 1.0$ the exponent value is $\alpha \simeq 2.0$.

panel (E) shows the dispersion with $\alpha \sim 1.47$ with inset showing the data in double logarithm. Panel (F) shows the similar results but for transverse phonons with $\alpha \sim 2.0$. Results obtained for polycrystalline solids are in close agreement with the results obtained for amorphous solids corroborate the robustness of an effective dynamical matrix description of the observation. Exponent $\alpha \sim 1.8$ for polycrystalline samples, quantitatively describe the divergence of MSD plateau with L as shown by solid curve in Fig.1(E). Similarly, if we choose $\alpha \sim 1.5$ for disordered solids, then we get $\delta \sim 1.0$ which is close to the exponent obtained from MD data. Further details are given in the SM.

In this section, we focus on the influence of long wavelength phonon modes on the dynamical heterogeneity (DH) in a system, as described by the four-point susceptibility, $\chi_4(t)$ [16]. Our analysis is based on the 2dmKA model, and we investigate how increasing activity affects the dynamical behavior of $\chi_4(t)$ for system sizes of $N = 4000$ and $N = 25000$ (shown in panels A and B of Fig.4). Panel (C) shows results for $\tau_p = 10$. Our findings indicate that increasing activity leads to the appearance

and enhancement of a short-time peak in $\chi_4(t)$, which becomes even more pronounced in two dimensions compared to three dimensions. Additionally, we observe the appearance of additional peaks or oscillations in $\chi_4(t)$, which are believed to be related to the higher harmonics of the frequencies. Interestingly, we find that the first peak of $\chi_4(t)$ diverges with system size (L), as reported for the 2D passive glass in previous studies [7]. However, the enhancement of this peak with increasing activity has not been reported before. In panel (B), we show that for larger system sizes, the first phonon peak starts to dominate over the peak at characteristic timescale, τ_α . At large enough activity and system size, the first peak becomes so large that it is hard to identify the existence of a peak at τ_α . Our results raise important questions about the measurement of DH in various experiments done in two dimensions with various forms of active driving, such as external vibration for granular medium, ATP-driven activity in biological systems, or chemical driving in chemophoretic particles. Even for Janus colloids, the effect will be much stronger due to the activity [6].

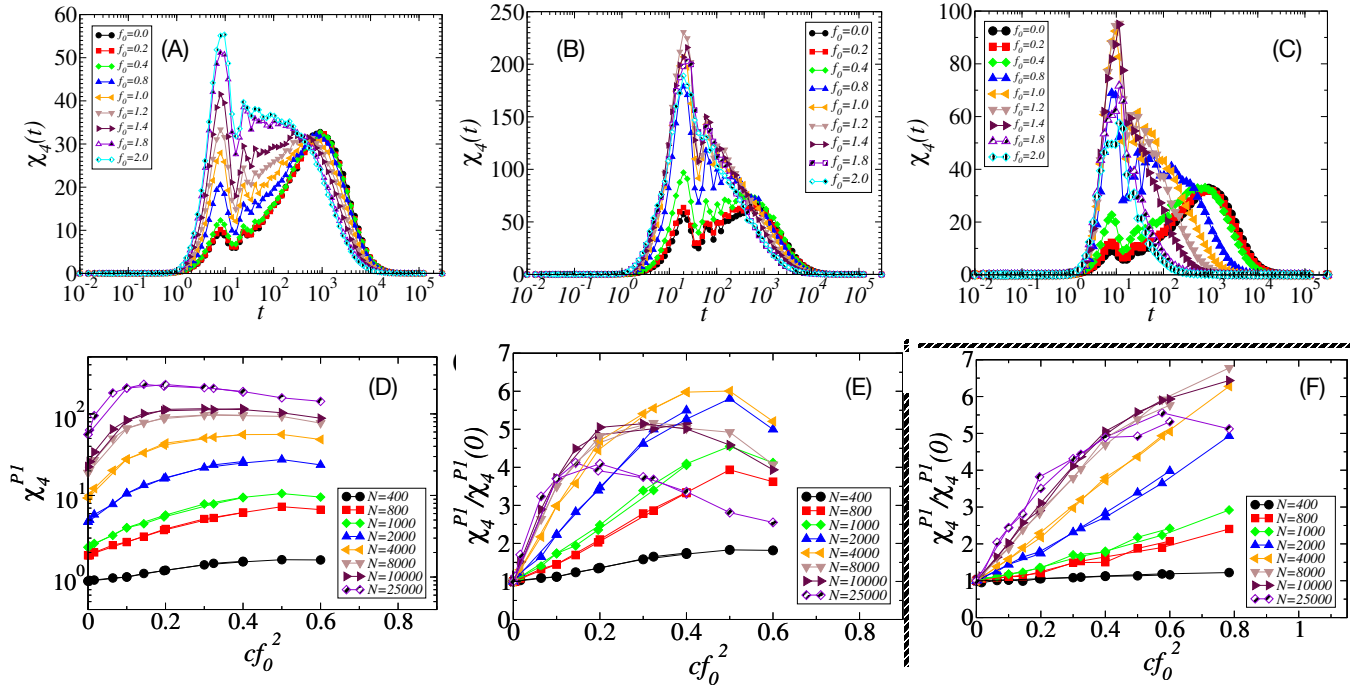


FIG. 4. (A), (B) and (C) shows $\chi_4(t)$ as function of time. (A) shows steady increase in first peak of $\chi_4(t)$ masking the $\chi_4(t)$ peak around τ_α for system size $N = 4000$ with changing activity f_0 , fixing $c = 0.1$ and $\tau_p = 1.0$, 2dmKA. (B) Same with $N = 25000$ keeping all parameters the same as (A), we can observe a drastic increase in the first χ_4 peak. (C) Results with $\tau_p = 10$. (D) χ_4^{P1} as function of effective activity cf_0^2 for 2dmKA system. (E) Scaled χ_4^{P1} with increasing activity with respect to the passive system. For 2dmKA system $\chi_4^{P1}/\chi_4^{P1}(0)$ shows saturation at some characteristic effective activity, which tends to decrease with increasing system size with a broader peak. (F) For 2dKA system $\chi_4^{P1}/\chi_4^{P1}(0)$ does not show a rapid decrease in characteristic activity with increasing system size like (E).

Fig.4(D) to (F) shows that first peak heights of $\chi_4(t)$ (referred as χ_4^{P1}) as a function of L for various f_0 with inset in panel (D) showing the results as a function of cf_0^2 which uniquely determines the degree of activity in the system. Interestingly, if we scale the zero activity value of the χ_4^{P1} for various system sizes, and plot the data as a function of cf_0^2 , then one finds that the curves tend to saturate to larger activity and in some cases they also tend to decrease giving rise to a broad peak at some characteristic activity especially for large system sizes. One also sees that the relative increase of χ_4^{P1} with increasing activity actually starts to become weaker as one increases system size for the 2dmKA model (see panel E), but it does not show a similar trend for the 2dKA model (see panel F). This surprising difference leads us to explore the possible effect of local ordering on these dynamical aspects of the systems.

Effect of Local Crystalline Order: In order to investigate the impact of activity on local ordering in disordered solids, we further examined the DH in 2dmKA and 2dKA models by eliminating the effect of long wavelength phonon modes. We achieved this by computing cage-relative correlation functions, as described in [9, 10, 43] and detailed in the Methods and SM. By computing $\chi_4^{P,CR}$ and τ_α^{CR} , we were able to isolate the structural part of the relaxation process. Cage-relative correlation

functions only consider the displacement of particles relative to their neighbouring particles or cage, thus eliminating the effect of long wavelength phonon modes in the calculations. In Fig.5(A), we present the cage-relative $\chi_4(t)$, or $\chi_4^{CR}(t)$, for the 2dmKA model system with increasing activity while keeping τ_p and c constant. We observe that the peak height of $\chi_4^{CR}(t)$ systematically decreases with increasing f_0 . In Fig.5(B), we show the variation of τ_α^{CR} as a function of f_0 for two different choices of τ_p . We observe that the relaxation time decreases monotonically with increasing activity. In panel (C) of the same figure, we plot $\chi_4^{P,CR}$ for the same conditions and note that DH decreases with increasing activity, as previously observed in various 3D systems [12]. In Fig.5(D), we present $\chi_4^{CR}(t)$ for the 2dKA model, which has prominent medium range crystalline order (MRCO) that increases with increasing supercooling. We observe that the peak height of $\chi_4^{CR}(t)$ increases with increasing activity, while the relaxation time decreases monotonically. This contrasts starkly with the 2dmKA model, which has no prominent local ordering in the studied temperature range. In panel (E), we plot τ_α^{CR} for three choices of $\tau_p = 1, 10, \text{ and } 100$. In all three cases, we observe that the relaxation time decreases monotonically with increasing f_0 . However, we note that the variation of $\chi_4^{P,CR}$ is different for these choices. For $\tau_p = 1$, the peak height re-

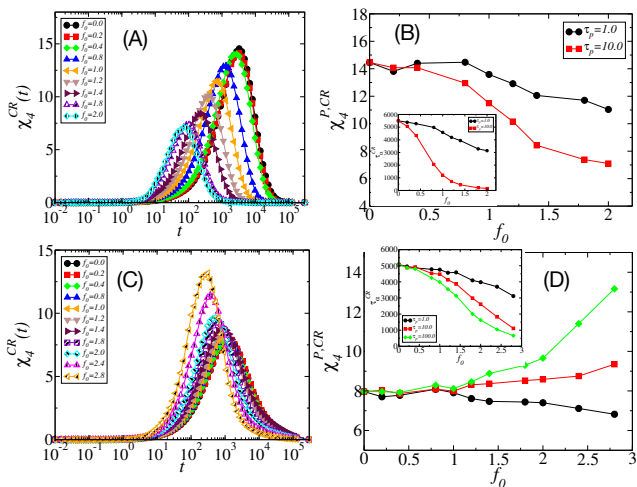


FIG. 5. (A) & (C) shows the cage-relative $\chi_4(t)$ as a function of time $N = 4000$ with changing f_0 . (A) is for 2dmKA model with $\tau_p = 10$ and (C) is for 2dKA model $\tau_p = 100$. Insets of (B) & (D) plots shows τ_α^{CR} vs f_0 , where in all the cases with increasing activity the τ_α^{CR} decreases. (B) & (D) shows $\chi_4^{P,CR}$ vs f_0 . In (C), $\chi_4^{P,CR}$ decreases with increasing activity for the 2dmKA model, but interestingly, in the plot (D), $\chi_4^{P,CR}$ shows an increasing trend beyond a certain threshold value of τ_p for 2dKA model.

mains nearly constant instead of decreasing, whereas for $\tau_p = 100$, we see a strong increase in peak height. These results suggest that activity enhances DH in all active supercooled liquids, but it does so differently for systems with local structural ordering. This is an important finding, as it implies that any observation of increasing $\chi_4(t)$ peak height with decreasing relaxation time in experimental systems in two dimensions might indicate hidden local ordering in the systems. Such systems would behave differently from those that do not tend to grow locally favoured structures (LFS). This observation might have implications for future studies, as it may allow us to quantify local order in various disordered systems and their role in glassy dynamics.

Motility Induced Mixing: Next, we focus on the structural analysis of two systems, namely 2dmKA and 2dKA models. First, we compute the displacement-displacement correlation function $\Gamma(r, \Delta t)$ (see SM for details) to evaluate the correlation between particle displacements computed over a time difference of Δt near the first peak of $\chi_4(t)$. We present the results of $\Gamma(r, \Delta t)$ for the 2dmKA model in Fig. 6(A), which shows that the correlation becomes longer range with increasing activity. We also compute the underlying correlation length by fitting the data to an exponential function. The growth of the correlation length with increasing activity is shown in the inset. Similar results for the 2dKA model system are presented in Fig. 6(B) and its inset. It is possible that activity leads to structural ordering in the system, resulting in longer-range spatial correlation, as predicted by the motility-induced phase separation (MIPS) scenario.

However, MIPS typically happens in dilute systems and not in dense limits. To investigate this further, we compute the local hexatic parameter, ψ_6 , and the corresponding spatial correlation of ψ_6 as $g_6(r) = \psi_6(0)\psi_6(r)$. In Fig. 6(C), we show the decay profile of $g_6(r)$ normalized by the radial distribution function $g(r)$. It is evident that the hexatic order does not increase with increasing f_0 as the spatial average of $\psi_6(r)$ for the 2dmKA model. Similar results for the 2dKA model are shown in Fig. 6(D). The average hexatic order also does not grow beyond its zero activity value of around 0.6. Interestingly, if we increase the persistent time τ_p , we observe that the hexatic order tends to get destroyed systematically, as illustrated in Fig. 6(E). The inset shows the decrease of mean hexatic order with increasing f_0 for $\tau_p = 100$, and Fig. 6(F) shows the snapshots of hexatic field maps for the cases $f_0 = 0.0$ (top) and $f_0 = 4.0$ (bottom). Thus, it seems that activity, especially with a larger persistence time, can lead to mixing instead of phase separation in dense systems with a strong tendency for crystallization. A detailed understanding of this interesting observation warrants more future investigations.

In Ref.[32], it was found that χ_4^P increases with activity even though τ_α decreases due to the over-expressing of RAB5A protein in confluent monolayer of MCF10A cells. Similarly, for the MRCO system, there is a drastic increase in $\chi_4^{P,CR}$ even when the τ_α^{CR} decreases. This effect is unique to the MRCO system, due to the presence of medium-range order and coloured noise above a certain threshold strength (τ_p), and is not observed in the normal (2dmKA) active glass or passive glass.

Brownian Dynamics Results: We performed Brownian Dynamics (BD) simulations to test the robustness of our observation that $\chi_4^{P,CR}$ increases with increasing activity despite the systematic decrease of relaxation time τ_α^{CR} . More details about these simulations can be found in the Methods section. In Fig.7, we presented $\chi_4(t)$ as a function of time for various activity strengths. We noticed that although the peak position, which represents the typical relaxation time of the system, decreases with increasing f_0 , the peak height consistently increases, thus confirming the validity of our MD results. It is important to note that we have only presented results for one model of an active system. It remains unclear whether the observed results are generic across various models of active particles like Active Brownian Particles (ABP), which is a question that needs further exploration. Additionally, we must bear in mind that overdamped Brownian particles are not significantly affected by long wavelength phonon modes even in passive systems due to the strong suppression of these modes in the presence of the system's internal frictions. However, the observation of MW fluctuations in experimental colloidal systems [6] suggests that activity in these systems will have much stronger MW fluctuations if measured carefully.

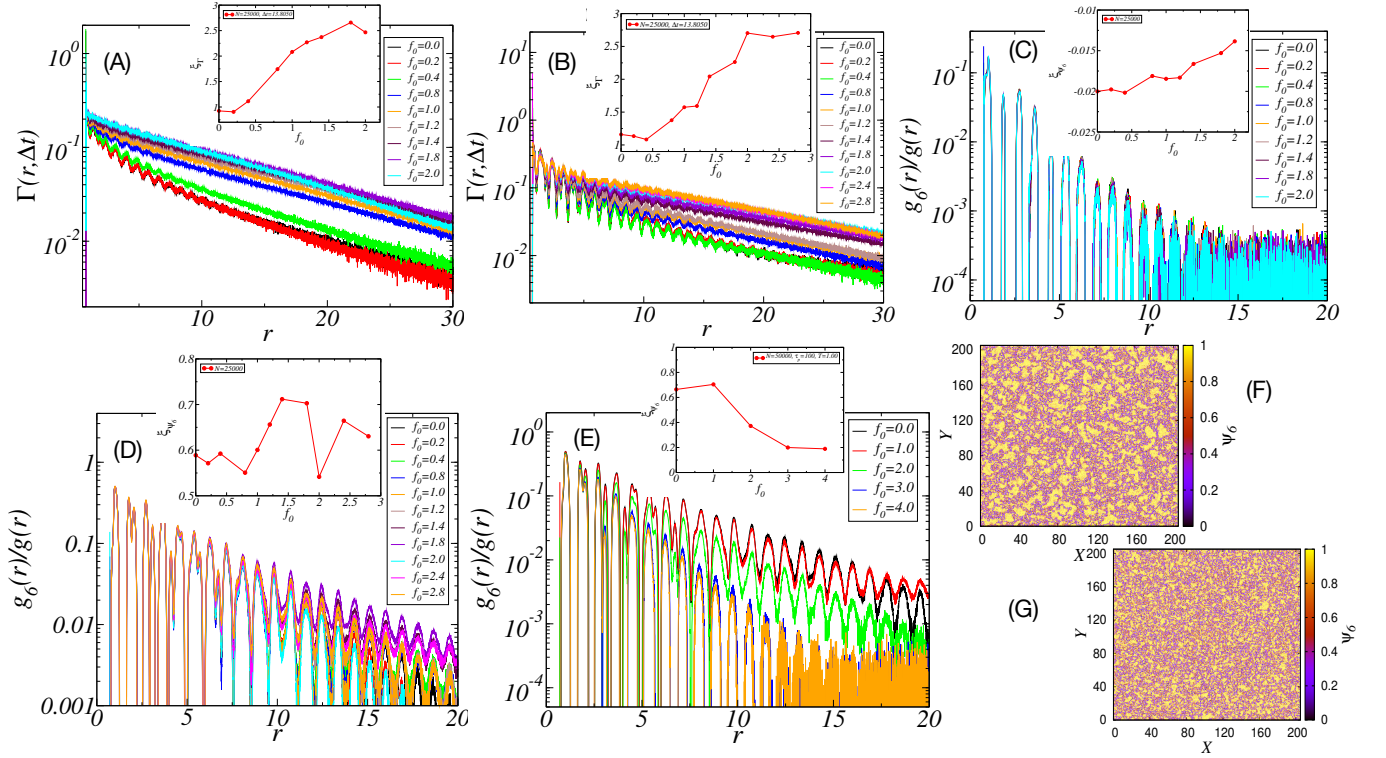


FIG. 6. Possible Motility Induced Phase Separation (MIPS): (A) & (B) Length scale ξ_r is extracted using excess displacement-displacement correlation ($\Gamma(r, \Delta t)$) calculation, where the ξ_r (Inset) shows increasing nature with activity up to a critical value, for (A) 2dmKA model, for (B) 2dKA model, $N = 25000$. (C) & (D) Length scale ξ_{ψ_6} (Inset) is extracted using relative hexatic correlation ($g_6(r)/g(r)$), which shows that activity does not lead to enhanced hexatic ordering in the system, (C) & (D) are for 2dmKA and 2dKA models respectively, $N = 25000$. (E) $g_6(r)/g(r)$ correlation starts to decrease with increasing activity for $\tau_p = 100$ for 2dKA model. Here ξ_{ψ_6} decreases at higher activity f_0 , $N = 50000$. Hexatic order parameter map for 2dKA model for (F) a passive system at $T = 1.0$ of system size and (G) at $f_0 = 4.0$, $c = 0.1$, $\tau_p = 100.0$, $T = 1.0$.

III. CONCLUSION

We conducted computer simulations to study the effect of long wavelength Mermin-Wagner type fluctuations in polycrystalline samples and two model glasses, one with local medium range crystalline order (MRCO) and the other without such predominant local structural motifs, in 2D. We found that active forces modelled as run-and-tumble (RTP) particles significantly enhance the local wavelength density fluctuations in these systems, causing a power-law divergence with system size (L) in the Debye-Waller (DW) factor. This exponent increases with increasing activity strength, universally in both crystalline and disordered solids. The long wavelength density fluctuations also affect high-temperature liquid dynamics, following results obtained in passive systems. We developed an effective dynamical matrix description of the observation by computing the effective Hessian matrix from displacement-displacement covariance matrix and performing exact diagonalization to compute the eigenvalues and eigenvectors. The obtained density of vibrational states (VDoS) matched very well for the passive systems after systematically correcting for convergence issues. VDoS results obtained following the same pro-

cedures led to the observation of enhanced phonon modes at lower frequencies with increasing activity, as evident from the appearance of sharp peaks in the distribution at small frequencies. The validity of this effective description was verified by computing the mean squared displacement (MSD) of particles in both crystals and amorphous solids using the detailed information of eigenvalues and eigenvectors of the effective Hessian matrix, showing close agreement with MD simulations results. Subsequently, to shed more light on the stronger than the logarithmic divergence of DW factors in crystalline and amorphous solids, we have computed the effective phonon dispersion relation and showed that in passive systems, one gets back the usual linear dispersion as $\omega(q) \sim q$, whereas in the presence of activity, this relation becomes non-linear as $\omega(q) \sim q^\alpha$, with exponent $\alpha \sim 1.8$ in polycrystalline solids and around $1.47 - 2.02$ in amorphous solids with exponent increasing systematically with increasing activity. These results qualitatively rationalize the observed power-law divergence of DW in crystalline and amorphous solids.

The effect of these MW phonon fluctuations on the dynamic heterogeneity in two studied model glasses also highlights how a naive dynamical measurement of four-

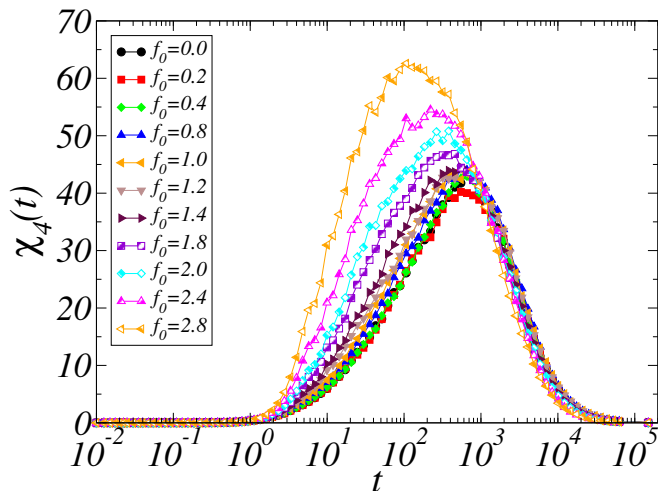


FIG. 7. $\chi_4(t)$ vs. t for different f_0 of system size $N = 50000$, at fixed $c = 0.1$, $\tau_p = 10.0$, using Brownian dynamic simulation for 2dKA model. Computation is done for a subsystem of size $L/3$ for better averaging (see Block Analysis section in SM).

point susceptibility, $\chi_4(t)$ in these systems in the presence of non-equilibrium active forces can lead to results which might be very counter-intuitive to understand, especially, the dramatic growth of an additional short-time peak in $\chi_4(t)$ with increasing activity can completely mask the long time peak due to the actual dynamical heterogeneity in these systems due to glassy dynamics. At the same time, we show that local structural ordering in these systems can have profound dynamical effects in the presence of active forces. For example, the 2dKA model, the model with local medium range crystalline order (MRCO), shows the increase of $\chi_4(t)$ peak with increasing activity even though the average characteristic relaxation time of the system is decreasing systematically. This starkly contrasts with the results obtained in the 2dmKA model, the model with no predominant local ordering, which shows a systematic decrease of $\chi_4(t)$ peak with increasing activity along with the monotonic decrease of the relaxation time. Note that in these computations, the effect of long-wavelength phonons has been systematically taken out by computing cage-relative correlation functions. These results might have a connection to a recent observation in Ref.[32] on a confluent monolayer of MCF10A cells, which showed a sharp increase of χ_4 peak although relaxation time decreases monotonically with increasing activity in the system. This suggests that the confluent monolayer might have local structural ordering although a very glass-like dynamical behaviour as in the case of the 2dKA model. A detailed investigation of the effect of local ordering and activity will be very interesting in the near future.

Finally, to comment on the non-universal nature of MW fluctuations in active systems, we highlight a recent result that demonstrated that the MW theorem is not valid in active systems, as MW fluctuations are strongly

suppressed, leading to true long-range crystalline ordering in 2D [44]. This is in line with the non-equilibrium disordered-to-order transition observed in the Vicsek model [18, 19, 21]. However, in our model active solids with RTP particles in two dimensions, we observe an opposite violation of the MW theorem. Our results suggest stronger MW fluctuations, rather than suppressed ones as in Ref.[44]. It appears that the details of how activity drives these self-propelled particles (SPPs) will significantly determine whether long-wavelength density fluctuations will be enhanced or suppressed. Our recent works [45, 46] suggest that the presence of RTP active particles gets strongly coupled to the global and local shear modes of relaxation, which are collective in nature, leading to faster annealing similar to the oscillatory shear response of these solids. We believe that the nature of active driving efficiently gets coupled to the local shear modes, leading to enhanced phonon-like fluctuations in the system. It will be interesting to investigate the effective phonon description in systems where activity suppresses the long wavelength density fluctuations as in Ref.[44]. Such studies may yield insight into whether the phonon dispersion changes consistently in those systems. However, our study will certainly motivate future research in these directions in two-dimensional active matters.

MATERIALS AND METHODS

Models & Simulation Details: In this work, we have studied the dynamics of crystalline and two model glass-forming liquids, respectively. The first glass-forming liquid model is the 2dmKA Binary model with a number ratio of 65 : 35 with the other details of the potential same as that of the Kob-Anderson model [47] (see SM for details). This particular number ratio ensures that there is no tendency for the system to form local crystalline orders. In contrast, the other model is referred to as a 2dKA binary mixture with 80 : 20 particle number ratio, and it forms local medium range crystalline order (MRCO) at low temperatures [48–50]. We have performed simulation $N \in [400, 10^5]$ in this work. We ran 32 statistically independent ensembles for all the systems except the few large ones (25000 – 10^5); we have taken 8 ensembles for these system sizes. The activity in the system is introduced in the form of run and tumble particle (RTP) dynamics [16, 17, 40], where the dynamics of the active particles can be tuned using three parameters such as c, f_0, τ_p . For setting up the reference temperature, we kept $\tau_p = 1$, active force magnitude f_0 is selected from 0.0 – 2.0 for 2dmKA and 0.0 – 2.8 for 2dKA by fixing concentration $c = 0.1$. When we varied the concentration $c \in [0.0, 0.6]$, we kept active force $f_0 = 1.0$ for both the 2dmKA and 2dKA systems. Due to the usage of the RTP motion of active particles, the inertial effect of the system is preserved; this will not be the case for the ABP (Active Brownian particle) model. Recent work on active matter suggests that the inertial term is important to

understand the system [51]. We used three-chain Noé-Hoover thermostat to perform NVT simulations [52]

Correlation Functions: To compute two-point density-density correlation, we have considered a simpler form of overlap correlation function $Q(t)$, such as

$$Q(t) = \frac{1}{N} \sum_{i=1}^N w(|\vec{r}_i(t) - \vec{r}_i(0)|). \quad (4)$$

where $w(x)$ is a window function, which is 1 for $x < a$ and 0 otherwise. $\vec{r}_i(t)$ position of the i^{th} at time t . Here parameter ‘a’ is chosen to remove the vibration due to the caging effect. We chose $a = 0.3$. Relaxation time, τ_α , which is defined as $\langle Q(t = \tau_\alpha) \rangle = 1/e$, where $\langle \dots \rangle >$ means ensemble average. The system is equilibrated for $150\tau_\alpha$, and then we run for $150\tau_\alpha$ in all our measurements. Four-point correlation function can be measured from the fluctuation of the two-point correlation function $Q(t)$, which is defined as,

$$\chi_4(t) = N \left[\langle Q(t)^2 \rangle - \langle Q(t) \rangle^2 \right]. \quad (5)$$

Mean Squared Displacement (MSD): The mean squared displacement (MSD) is defined as

$$\langle \Delta r^2(t) \rangle = \frac{1}{N} \sum_{i=1}^N |\vec{r}_i(t) - \vec{r}_i(0)|^2, \quad (6)$$

Cage-relative Displacement: The cage-relative (CR) displacement [9, 10, 43] of the individual particle i , is defined as

$$\vec{r}_{i,CR}(t) = [\vec{r}_i(t) - (\vec{r}_{i,nn}(t) - \vec{r}_{i,nn}(0))] \quad (7)$$

where $\vec{r}_{i,nn}(t)$ is the position of the center of mass of N_{nn} nearest neighbours of i^{th} particles. Again it is defined as,

$$\vec{r}_{i,nn}(t) = \frac{1}{N_{nn}} \sum_{j=1}^{N_{nn}} [\vec{r}_j(t) - \vec{r}_j(0)]. \quad (8)$$

We used cut-off value $r_c^{nn} = 1.3$ for the first nearest neighbours N_{nn} . After identifying the N_{nn} particles at the initial time (time origin) we track these particles dynamics at later time t . Using these displacement we compute $Q^{CR}(t)$, $\chi_4^{CR}(t)$, and MSD respectively.

Hessian Matrix (\mathcal{H}): The Hessian matrix is defined as the double derivative of the total potential energy, $U(\{\vec{r}_i\})$, as

$$\mathcal{H}_{ij}^{\alpha\beta} = \frac{\partial^2 U(\{\vec{r}_i\})}{\partial r_i^\alpha \partial r_i^\beta}, \quad (9)$$

with i, j being the particle index and α, β being the dimensionality index.

-
- [1] N. D. Mermin and H. Wagner. Absence of ferromagnetism or antiferromagnetism in one- or two-dimensional isotropic heisenberg models. *Phys. Rev. Lett.*, 17(22):1133–1136, November 1966.
- [2] N. D. Mermin. Crystalline order in two dimensions. *Phys. Rev.*, 176(1):250–254, December 1968.
- [3] J M Kosterlitz and D J Thouless. Ordering, metastability and phase transitions in two-dimensional systems. *Journal of Physics C: Solid State Physics*, 6(7):1181–1203, April 1973.
- [4] B. I. Halperin and David R. Nelson. Theory of two-dimensional melting. *Phys. Rev. Lett.*, 41(2):121–124, July 1978.
- [5] A. P. Young. Melting and the vector coulomb gas in two dimensions. *Phys. Rev. B*, 19(4):1855–1866, February 1979.
- [6] Yan-Wei Li, Chandan K. Mishra, Zhao-Yan Sun, Kun Zhao, Thomas G. Mason, Rajesh Ganapathy, and Massimo Pica Ciamarra. Long-wavelength fluctuations and anomalous dynamics in 2-dimensional liquids. *Proc. Nat. Acad. of Sci. (USA)*, 116(46):22977–22982, October 2019.
- [7] Hayato Shiba, Yasunori Yamada, Takeshi Kawasaki, and Kang Kim. Unveiling dimensionality dependence of glassy dynamics: 2d infinite fluctuation eclipses inherent structural relaxation. *Phys. Rev. Lett.*, 117(24):245701, December 2016.
- [8] Elijah Flenner and Grzegorz Szamel. Fundamental differences between glassy dynamics in two and three dimensions. *Nat. Commun.*, 6(1), June 2015.
- [9] Skanda Vivek, Colm P. Kelleher, Paul M. Chaikin, and Eric R. Weeks. Long-wavelength fluctuations and the glass transition in two dimensions and three dimensions. *Proc. Nat. Acad. of Sci. (USA)*, 114(8):1850–1855, January 2017.
- [10] Bernd Illing, Sebastian Fritschi, Herbert Kaiser, Christian L. Klix, Georg Maret, and Peter Keim. Mermin-wagner fluctuations in 2d amorphous solids. *Proc. Nat. Acad. of Sci. (USA)*, 114(8):1856–1861, January 2017.
- [11] Zane Shi, Pablo G Debenedetti, and Frank H Stillinger. Relaxation processes in liquids: Variations on a theme by stokes and einstein. *The Journal of chemical physics*, 138(12), 2013.
- [12] Kallol Paul, Anoop Mutneja, Saroj Kumar Nandi, and Smarajit Karmakar. Dynamical heterogeneity in active glasses is inherently different from its equilibrium behavior. *Proc. Nat. Acad. of Sci. (USA)*, 120(34), August 2023.
- [13] Andrea Cavagna. Supercooled liquids for pedestrians. *Physics Reports*, 476(4-6):51–124, June 2009.
- [14] Ludovic Berthier and Giulio Biroli. Theoretical perspective on the glass transition and amorphous materials. *Rev. Mod. Phys.*, 83(2):587–645, June 2011.
- [15] Smarajit Karmakar, Chandan Dasgupta, and Srikanth Sastry. Growing length scales and their relation to timescales in glass-forming liquids. *Ann. Rev. of Condens. Matt. Phys.*, 5(1):255–284, March 2014.

- [16] Subhdeep Dey, Anoop Mutneja, and Smarajit Karmakar. Enhanced short time peak in four-point dynamic susceptibility in dense active glass-forming liquids. *Soft Matter*, 18(38):7309–7316, 2022.
- [17] Rituparno Mandal, Pranab Jyoti Bhuyan, Madan Rao, and Chandan Dasgupta. Active fluidization in dense glassy systems. *Soft Matter*, 12(29):6268–6276, 2016.
- [18] Tamás Vicsek, András Czirók, Eshel Ben-Jacob, Inon Cohen, and Ofer Shochet. Novel type of phase transition in a system of self-driven particles. *Phys. Rev. Lett.*, 75(6):1226–1229, August 1995.
- [19] John Toner and Yuhai Tu. Flocks, herds, and schools: A quantitative theory of flocking. *Phys. Rev. E*, 58(4):4828–4858, October 1998.
- [20] Sriram Ramaswamy. The mechanics and statistics of active matter. *Ann. Rev. of Condens. Matt. Phys.*, 1(1):323–345, August 2010.
- [21] Jeremie Palacci, Stefano Sacanna, Asher Preska Steinberg, David J. Pine, and Paul M. Chaikin. Living crystals of light-activated colloidal surfers. *Science*, 339(6122):936–940, February 2013.
- [22] M. C. Marchetti, J. F. Joanny, S. Ramaswamy, T. B. Liverpool, J. Prost, Madan Rao, and R. Aditi Simha. Hydrodynamics of soft active matter. *Rev. Mod. Phys.*, 85(3):1143–1189, July 2013.
- [23] E. H. Zhou, X. Trepát, C. Y. Park, G. Lenormand, M. N. Oliver, S. M. Mijailovich, C. Hardin, D. A. Weitz, J. P. Butler, and J. J. Fredberg. Universal behavior of the osmotically compressed cell and its analogy to the colloidal glass transition. *Proc. Nat. Acad. of Sci. (USA)*, 106(26):10632–10637, June 2009.
- [24] Thomas E. Angelini, Edouard Hannezo, Xavier Trepát, Manuel Marquez, Jeffrey J. Fredberg, and David A. Weitz. Glass-like dynamics of collective cell migration. *Proc. Nat. Acad. of Sci. (USA)*, 108(12):4714–4719, February 2011.
- [25] Bradley R. Parry, Ivan V. Surovtsev, Matthew T. Cabeen, Corey S. O’Hern, Eric R. Dufresne, and Christine Jacobs-Wagner. The bacterial cytoplasm has glass-like properties and is fluidized by metabolic activity. *Cell*, 156(1-2):183–194, January 2014.
- [26] Jin-Ah Park, Jae Hun Kim, Dapeng Bi, Jennifer A. Mitchel, Nader Taheri Qazvini, Kelan Tantisira, Chan Young Park, Maureen McGill, Sae-Hoon Kim, Bomi Gweon, Jacob Notbohm, Robert Steward Jr, Stephanie Burger, Scott H. Randell, Alvin T. Kho, Dhananjay T. Tambe, Corey Hardin, Stephanie A. Shore, Elliot Israel, David A. Weitz, Daniel J. Tschumperlin, Elizabeth P. Henske, Scott T. Weiss, M. Lisa Manning, James P. Butler, Jeffrey M. Drazen, and Jeffrey J. Fredberg. Unjamming and cell shape in the asthmatic airway epithelium. *Nat. Mat.*, 14(10):1040–1048, August 2015.
- [27] Simon Garcia, Edouard Hannezo, Jens Elgeti, Jean-François Joanny, Pascal Silberzan, and Nir S. Gov. Physics of active jamming during collective cellular motion in a monolayer. *Proc. Nat. Acad. of Sci. (USA)*, 112(50):15314–15319, December 2015.
- [28] Chiara Malinverno, Salvatore Corallino, Fabio Giavazzi, Martin Bergert, Qingsen Li, Marco Leoni, Andrea Disanza, Emanuela Frittoli, Amanda Oldani, Emanuele Martini, Tobias Lendenmann, Gianluca Deflorian, Galina V. Beznoussenko, Dimos Poulidakos, Kok Haur Ong, Marina Uroz, Xavier Trepát, Dario Parazzoli, Paolo Maiuri, Weimiao Yu, Aldo Ferrari, Roberto Cerbino, and Giorgio Scita. Endocytic reawakening of motility in jammed epithelia. *Nat. Mat.*, 16(5):587–596, January 2017.
- [29] Kenji Nishizawa, Kei Fujiwara, Masahiro Ikenaga, Nobushige Nakajo, Miho Yanagisawa, and Daisuke Mizuno. Universal glass-forming behavior of in vitro and living cytoplasm. *Scientific Reports*, 7(1), November 2017.
- [30] Jae Hun Kim, Adrian F. Pegoraro, Amit Das, Stephan A. Koehler, Sylvia Ann Ujwary, Bo Lan, Jennifer A. Mitchel, Lior Atia, Shijie He, Karin Wang, Dapeng Bi, Muhammad H. Zaman, Jin-Ah Park, James P. Butler, Kyu Ha Lee, Jacqueline R. Starr, and Jeffrey J. Fredberg. Unjamming and collective migration in MCF10a breast cancer cell lines. *Biochemical and Biophysical Research Communications*, 521(3):706–715, January 2020.
- [31] Medhavi Vishwakarma, Basil Thurakkal, Joachim P. Spatz, and Tamal Das. Dynamic heterogeneity influences the leader–follower dynamics during epithelial wound closure. *Philosophical Transactions of the Royal Society B: Biological Sciences*, 375(1807):20190391, July 2020.
- [32] Roberto Cerbino, Stefano Villa, Andrea Palamidessi, Emanuela Frittoli, Giorgio Scita, and Fabio Giavazzi. Disentangling collective motion and local rearrangements in 2d and 3d cell assemblies. *Soft Matter*, 17(13):3550–3559, 2021.
- [33] Étienne Fodor, Cesare Nardini, Michael E. Cates, Julien Tailleur, Paolo Visco, and Frédéric van Wijland. How far from equilibrium is active matter? *Phys. Rev. L*, 117(3), July 2016.
- [34] Saroj Kumar Nandi, Rituparno Mandal, Pranab Jyoti Bhuyan, Chandan Dasgupta, Madan Rao, and Nir S. Gov. A random first-order transition theory for an active glass. *Proc. Nat. Acad. of Sci. (USA)*, 115(30):7688–7693, July 2018.
- [35] Ludovic Berthier and Jorge Kurchan. Non-equilibrium glass transitions in driven and active matter. *Nat. Phys.*, 9(5):310–314, March 2013.
- [36] Ludovic Berthier. Nonequilibrium glassy dynamics of self-propelled hard disks. *Phys. Rev. Lett.*, 112(22):220602, June 2014.
- [37] Ran Ni, Martien A. Cohen Stuart, and Marjolein Dijkstra. Pushing the glass transition towards random close packing using self-propelled hard spheres. *Nat. Commun.*, 4(1), October 2013.
- [38] Saroj Kumar Nandi and Nir S. Gov. Nonequilibrium mode-coupling theory for dense active systems of self-propelled particles. *Soft Matter*, 13(41):7609–7616, 2017.
- [39] Ludovic Berthier, Elijah Flenner, and Grzegorz Szamel. Glassy dynamics in dense systems of active particles. *The Journal of Chemical Physics*, 150(20):200901, May 2019.
- [40] Kallol Paul, Anoop Mutneja, Saroj Kumar Nandi, and Smarajit Karmakar. Dynamical heterogeneity in active glasses is inherently different from its equilibrium behavior, 2021.
- [41] Ke Chen, Tim Still, Samuel Schoenholz, Kevin B. Aptowicz, Michael Schindler, A. C. Maggs, Andrea J. Liu, and A. G. Yodh. Phonons in two-dimensional soft colloidal crystals. *Phys. Rev. E*, 88(2), August 2013.
- [42] Tim Still, Carl P. Goodrich, Ke Chen, Peter J. Yunker, Samuel Schoenholz, Andrea J. Liu, and A. G. Yodh. Phonon dispersion and elastic moduli of two-dimensional disordered colloidal packings of soft particles with fric-

- tional interactions. *Phys. Rev. E*, 89(1), January 2014.
- [43] S. Mazoyer, F. Ebert, G. Maret, and P. Keim. Dynamics of particles and cages in an experimental 2d glass former. *EPL (Europhysics Letters)*, 88(6):66004, December 2009.
- [44] Leonardo Galliano, Michael E. Cates, and Ludovic Berthier. Two-dimensional crystals far from equilibrium. *Phys. Rev. L*, 131(4), July 2023.
- [45] Umang A. Dattani, Rishabh Sharma, Smarajit Karmakar, and Pinaki Chaudhuri. Cavitation instabilities in amorphous solids via secondary mechanical perturbations, 2023.
- [46] Rishabh Sharma and Smarajit Karmakar. Activity-induced annealing leads to ductile-to-brittle transition in amorphous solids, 2023.
- [47] Rajsekhar Das, Saurish Chakrabarty, and Smarajit Karmakar. Pinning susceptibility: a novel method to study growth of amorphous order in glass-forming liquids. *Soft Matter*, 13(38):6929–6937, 2017.
- [48] Takeshi Kawasaki, Takeaki Araki, and Hajime Tanaka. Correlation between dynamic heterogeneity and medium-range order in two-dimensional glass-forming liquids. *Phys. Rev. L*, 99(21), November 2007.
- [49] Hajime Tanaka, Takeshi Kawasaki, Hiroshi Shintani, and Keiji Watanabe. Critical-like behaviour of glass-forming liquids. *Nat. Mat.*, 9(4):324–331, February 2010.
- [50] Indrajit Tah, Shiladitya Sengupta, Srikanth Sastry, Chandan Dasgupta, and Smarajit Karmakar. Glass transition in supercooled liquids with medium-range crystalline order. *Phys. Rev. Lett.*, 121(8):085703, August 2018.
- [51] Michael te Vrugt, Tobias Frohoff-Hülsmann, Eyal Heifetz, Uwe Thiele, and Raphael Wittkowski. From a microscopic inertial active matter model to the schrödinger equation. *Nat. Commun.*, 14(1), March 2023.
- [52] Glenn J. Martyna, Michael L. Klein, and Mark Tuckerman. Nosé–hoover chains: The canonical ensemble via continuous dynamics. *The Journal of Chemical Physics*, 97(4):2635–2643, August 1992.

Supplementary Information : Enhanced Long Wavelength Mermin-Wagner Fluctuations in Two-Dimensional Active Crystals and Glasses

Subhodeep Dey, Antik Bhattacharya, and Smarajit Karmakar*
 Tata Institute of Fundamental Research Hyderabad,
 36/P, Gopanpally Village, Serilingampally Mandal,
 Ranga Reddy District, Hyderabad, Telangana 500046, India.

I. MODELS AND METHODS

In this study, we have used a Binary Mixture of particles, which interact via well-known Lennard-Jones (LJ) potential. This potential has been tuned such that the 2nd derivative of the potential is smoothed up to the cut-off distance r_c ,

$$\phi(r) = \begin{cases} 4\epsilon_{\alpha\beta} \left[\left(\frac{\sigma_{\alpha\beta}}{r} \right)^{12} - \left(\frac{\sigma_{\alpha\beta}}{r} \right)^6 + c_0 + c_2 r^2 \right] & , r < r_c \\ 0 & , r \geq r_c \end{cases} \quad (1)$$

Here, $\{\alpha, \beta\}$ refers to the type of the particles, which can be A (large) or B (small) type. We studied two types of glass-forming liquids; one is 2D modified Kob-Andersen (2dmKA), where A:B number ratio is 65 : 35, and other one is 2D Kob-Andersen model (2dKA), where A:B number ratio is 80 : 20 [1]. The interaction strengths are $\epsilon_{AA} = 1.0$, $\epsilon_{AB} = 1.5$, $\epsilon_{BB} = 0.5$ and the diameter of the particles are $\sigma_{AA} = 1.0$, $\sigma_{AB} = 0.8$, $\sigma_{BB} = 0.88$. The interaction cut-off is $r_c = 2.5\sigma_{AB}$. Here the reduced unit of length, energy and time are given by σ_{AA} , ϵ_{AA} and $\sqrt{\frac{\sigma_{AA}^2}{\epsilon_{AA}}}$ respectively. For all cases, the system's particle density (ρ) is fixed at 1.2, and the integration step (δt) is set at 0.005. For polycrystal simulations, we used only A-type particles at a density of 1.2, and for the integration step here, we also kept the same $\delta t = 0.005$.

II. ACTIVITY IN THE SYSTEM: RUN AND TUMBLE PARTICLE (RTP) MODEL

To introduce activity in the system, we have given additional active force, f_0 , to a set of selected (tagged) active particles in addition to their mutual particle-particle interaction coming from the inter-particle potential. Here, we have selected fraction (c) of active particles in the system. We assign each active particle a active direction (k_x, k_y) randomly in a manner that the total active force applied to all the active particles sum up to zero. This done to maintain the momentum conservation in the system. The persistent time τ_p is the time until which the active force on each particle acts in the same direction and after τ_p , the directions are randomly

reshuffled. The active force on the i^{th} particle in 2D can be written as,

$$\vec{F}_i^A = f_0(k_x^i \hat{x} + k_y^i \hat{y}), \quad (2)$$

where the active direction (kx, ky) is chosen from ± 1 , and the number of total active particles is taken to be an even number to maintain the total active momentum to be zero along all directions, i.e., $\sum_{\alpha, i} k_\alpha^i = 0$. Now, in this active system, there are three tuning parameters c , f_0 and τ_p . We have different activity parameters for 2dmKA and 2dKA systems depending on the activity limit. To start with, we first fixed $\tau_p = 1.0$ for all the cases, then we changed the f_0 and c separately. For 2dmKA, we have varied $f_0 \in [0.0-2.0]$, and for 2dKA, we have varied $f_0 \in [0.0-2.8]$, keeping c fixed at 0.1 for both cases. Again, for both 2dmKA and 2dKA, while varying $c \in [0.1-0.6]$, we kept f_0 fixed at 1.0. Later, to study the effect of persistent time, we have varied f_0 at $\tau_p = 10$ and 100 at fixed $c = 0.1$.

III. THERMOSTAT

In this study, we have used the three-chain Nosé-Hoover thermostat [2] to get the required temperature. This thermostat is known to give a true canonical ensemble in an equilibrium system, which is also suitable for a canonical ensemble in an out-of-equilibrium system. Here, we have taken the coupling relaxation time (τ_T) of the thermostat 10 times the integration time step (δt).

IV. TWO-POINT CORRELATION FUNCTION, $Q(t)$

To compute two-point density-density correlation, we have considered a simpler form of overlap correlation function $Q(t)$ defined as

$$Q(t) = \frac{1}{N} \sum_{i=1}^N w(|\vec{r}_i(t) - \vec{r}_i(0)|), \quad (3)$$

where $w(x)$ is a window function, which is 1 for $x < a$ and 0 otherwise. $\vec{r}_i(t)$ is the position of the i^{th} at time t . Here, parameter 'a' is chosen to remove the vibration due to the caging effect. One can choose the value of 'a' from the plateau of a 'mean-square displacement' (MSD) in the supercooled temperature regime. For all

* smarajit@tifrh.res.in

cases, the value of a is set to 0.3. From this two-point correlation function, we define a relaxation time τ_α , as $\langle Q(t = \tau_\alpha) \rangle = 1/e$, where $\langle \dots \rangle$ is ensemble average and e is the base of the natural logarithm. The system is equilibrated for $150\tau_\alpha$ and then we ran the simulations for another $150\tau_\alpha$ for measuring various dynamical and thermodynamic quantities. We chose $\tau_\alpha \sim 2000$. For system size $N \leq 10000$, we have averaged our data over 32 statistically independent ensembles runs, and for system size $N > 10000$, we have taken 6 ensembles for averaging.

V. FOUR-POINT CORRELATION FUNCTION, $\chi_4(t)$

The four-point correlation function can be measured from the fluctuation of the two-point correlation function $Q(t)$ as,

$$\chi_4(t) = N \left[\langle Q(t)^2 \rangle - \langle Q(t) \rangle^2 \right], \quad (4)$$

where $\langle \dots \rangle$ is the ensemble average. $\chi_4(t)$ is a well-known quantifier of dynamic heterogeneity (DH) in the system. Dynamic heterogeneity broadly refers to the heterogeneous dynamical relaxation processes in various parts of the system. This happens due to different population of slow and fast-moving particles in the system. DH reaches its maximum round the relaxation time τ_α and the peak is defined as $\chi_4(t = \tau_\alpha) \simeq \chi_4^P$. In this study, due to the activity and increasing system size, one observes the emergence of an additional peak at the early-beta regime in $\chi_4(t)$. We focus on the first peak of the $\chi_4(t)$ in the early-beta regime and define the first peak as $\chi_4(t = t^*) \simeq \chi_4^{P1}$, where t^* is the characteristic time at which the first peak appears.

VI. CAGE-RELATIVE DISPLACEMENT

At large system size limit with increasing activity, the system starts to show increasing fluctuations at the short time of $\chi_4(t)$. The fluctuations becomes so large that it nearly mask the heterogeneity peak χ_4^P around relaxation time τ_α . To separate the influence of the collective behaviour affecting the system dynamics due to glassy relaxation process and not from the long wavelength phonon fluctuations, we have computed the cage-relative (CR) displacement [3–5] of the individual particle i , such as

$$\vec{r}_{i,CR}(t) = [\vec{r}_i(t) - (\vec{r}_{i,nn}(t) - \vec{r}_{i,nn}(0))], \quad (5)$$

where $\vec{r}_{i,nn}(t)$ is the position of the center of mass of N_{nn} nearest neighbours of i^{th} particles. Again it is defined as

$$\vec{r}_{i,nn}(t) = \frac{1}{N_{nn}} \sum_{j=1}^{N_{nn}} [\vec{r}_j(t) - \vec{r}_j(0)]. \quad (6)$$

Here, we have used cut-off value $r_c^{nn} = 1.3$ for the first nearest neighbours N_{nn} . After identifying the N_{nn} particles at the initial time or at each time origin, we track these particles' (N_{nn}) dynamics at the later time for the computation of the cage relative correlation functions. We use this cage-relative displacement to calculate $Q(t)$, $\chi_4(t)$ and MSD, respectively.

VII. CHOICE OF TEMPERATURE FOR DIFFERENT ACTIVITY

As activity in each model (2dmKA and 2dKA) can be tuned either by tuning the fraction of active particles (c) or the active force (f_0) or the persistent time (τ_p), it is important to identify a correct measure to compare these systems across the parameter space. For this we choose relaxation time τ_α is the system's characteristics for comparison across various values of c , f_0 and τ_p . For a given set of c , f_0 and τ_p , if we vary T , then the obtained relaxation time is found to obey the well-known 'Vogel-Fulcher-Tammann' (VFT) relation, defined as

$$\tau_\alpha = \tau_0 \exp[A/T - T_0]. \quad (7)$$

We then take an intermediate system size and fix the τ_α for different activities at the suitable temperature using the VFT relation. For 2dmKA, we have taken the relaxation time $\tau_\alpha \simeq 2400$ which happens at $T = 0.43$ of a passive system with $N = 1000$. We then fix these temperatures for all other system sizes for a direct comparison. For 2dmKA model system, we firstly change the f_0 from 0.0 to 2.0 by fixing $c = 0.1$ and $\tau_p = 1.0$. Next, we have changed the c from 0.0 to 0.6 by fixing $f_0 = 1.0$ and $\tau_p = 1.0$. Similarly, for 2dKA, we have taken the relaxation time $\tau_\alpha \simeq 2200$ at $T = 1.00$ of a passive system with $N = 1000$ and fixed it for all other activities and system sizes. We changed the values of f_0 from 0.0 to 2.8 by fixing $c = 0.1$ with $\tau_p = 1.0$. Then, we change the c from 0.0 to 0.6 by fixing $f_0 = 1.0$ and $\tau_p = 1.0$. From Fig. 1, we have used the temperature for the respective activity parameter and fixed it for the rest of the study. Again, in Fig. 2, we have shown that the choice of temperature corresponding to different activity is giving similar relaxation time for the system size $N = 1000$.

VIII. LARGE SYSTEM SIZE IN HIGH ACTIVITY LIMIT

To understand the effect of changing f_0 in the high persistent time limit ($\tau_\alpha = 10$ and 100), we have taken large system $N = 50000$ for 2dKA model simulations. Fig. 3 shows that the $\chi_4^{P,CR}$ starts to increase from activity $f_0 = 2.0$, where at small activity limit $\chi_4^{P,CR}$ fluctuates around 7 and 8. To see the effect of activity alone, we have fixed the system as high-temperature $T=1.100$ for all activity. From Fig. 4 we observe that there is no

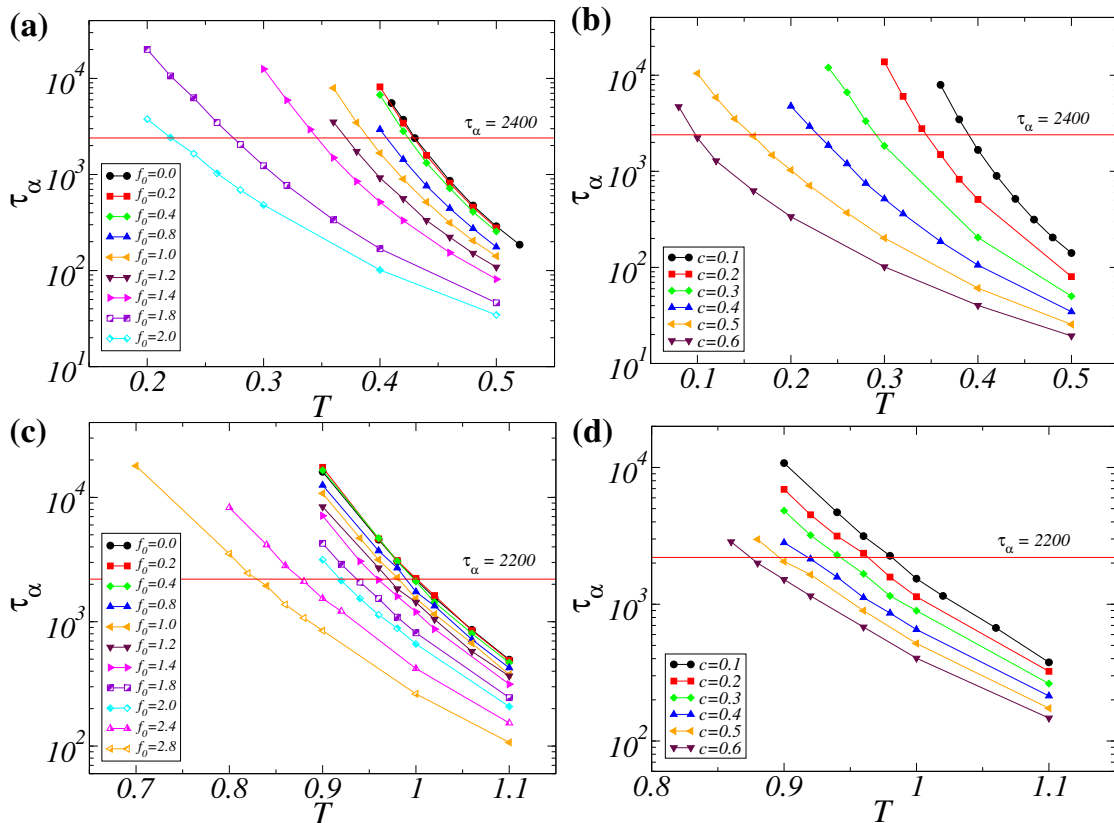


FIG. 1. Left panel: (a) & (c) plots represents τ_α vs T for different f_0 and fixed $c=0.1$ and $\tau_p = 1.0$. Right panel: (b) & (d) plots represents τ_α vs T for different c and fixed $f_0 = 1.0$ and $\tau_p = 1.0$. Top panel: (a), (b) plots are for the 2dmKA model and bottom panel: (c), (d) plots are for the 2dKA model.

clear trend of increasing $\chi_4^{P,CR}$ with increasing activity, it fluctuates around 6 to 8 for different activity. Both observations show that $\chi_4^{P,CR}$ does not decrease with increasing activity even at very low τ_α . We observe an additional peak arising for small activity at a long time limit; this effect could be due to less averaging at a longer time.

IX. BLOCK ANALYSIS

To study the effect of other fluctuations including number, density, composition, temperature and activity fluctuations, we used the method of Block Analysis as detailed in Ref.[6], where one divides the whole system into multiple subsystems of equal linear sizes and then computes the relevant correlation functions. This method is very useful for colloidal experiments, in which often one records the data over a small measurement region in the whole sample. The two-point correlation for a single subsystem can be defined as,

$$Q(L_B, t) = \frac{1}{n_i} \sum_{j=1}^{n_i} [w(r_j(t) - r_j(0))], \quad (8)$$

where $L_B = (N/N_B)^{1/3}$ is the subsystem size, N_B is the number of subsystems (blocks) and n_i is the number of particles in the i^{th} block. The average two-point correlation function is given by,

$$\langle Q(L_B, t) \rangle = \frac{1}{N_B} \sum_{i=1}^{N_B} Q(L_B, t). \quad (9)$$

Similarly, the four-point dynamic susceptibility for each block can be computed as,

$$\chi'_4(L_B, t) = \left[\langle Q(L_B, t)^2 \rangle - \langle Q(L_B, t) \rangle^2 \right]. \quad (10)$$

The system averaged four-point dynamic susceptibility of the sub-system (L_B) is given by,

$$\chi_4(L_B, t) = \left(\frac{N}{N_B} \right) [\chi'_4(L_B, t)]. \quad (11)$$

Here $\langle \dots \rangle$ denotes the average over different grand-canonical ensembles, i.e., for different time origins and sub-systems.

X. BROWNIAN DYNAMICS

We have also performed Brownian dynamics (BD) simulations [7] to understand the effect of activity in over-

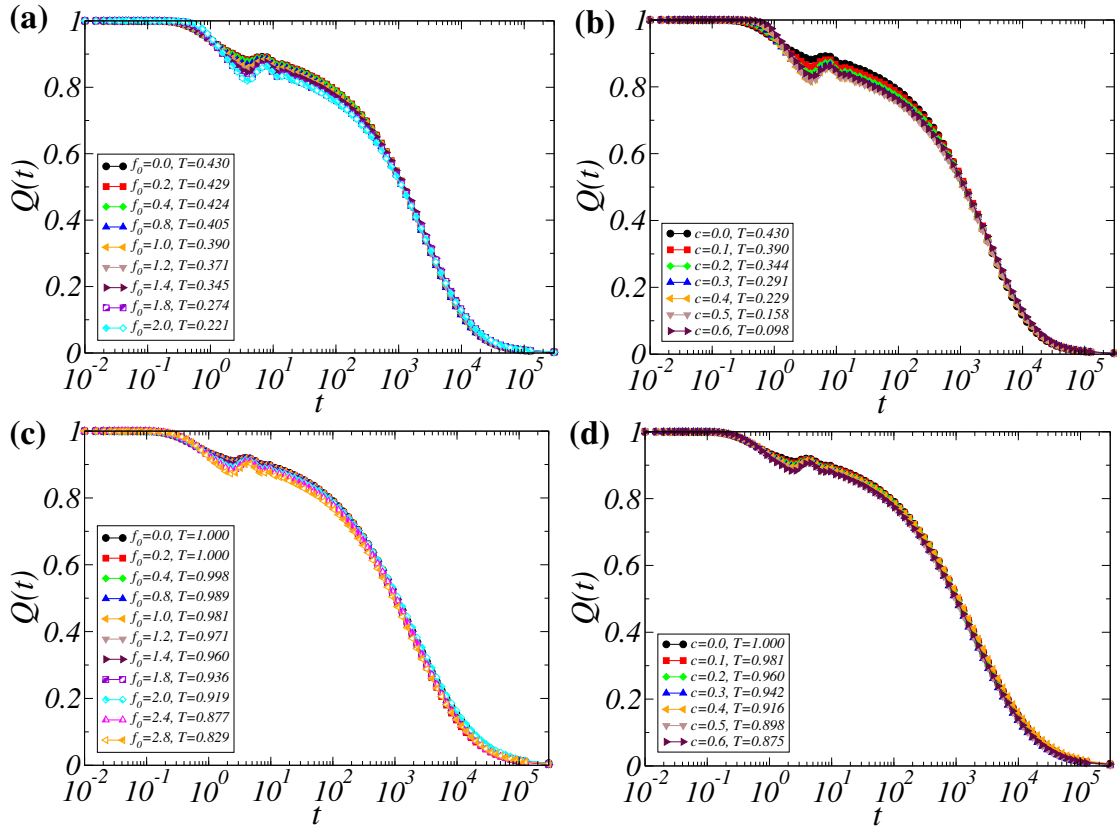


FIG. 2. Left panel: (a) & (c) plots represent two-point correlation vs for different f_0 at fixed $c=0.1$, $\tau_p = 1.0$ gives similar relaxation time. Right panel: (b) & (d) plots represent two-point correlation vs for different c at fixed $f_0 = 1.0$, $\tau_p = 1.0$ gives similar relaxation time. Top panel: (a), (b) plots are for the 2dmKA model and bottom panel: (c), (d) plots are for the 2dKA model.

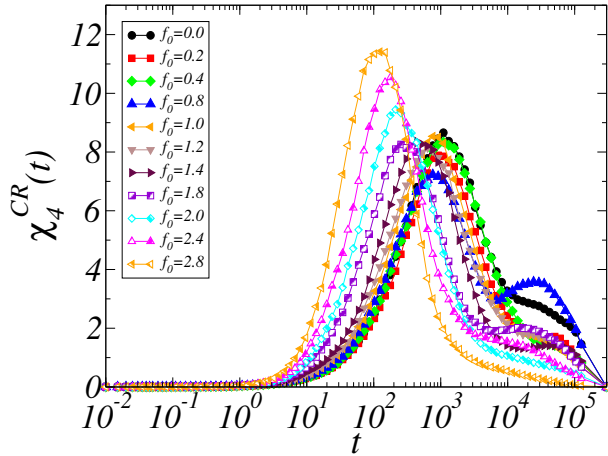


FIG. 3. ($\chi_4^{CR}(t)$ vs. t) for different f_0 of system size $N=50000$, at fixed $c=0.1$, $\tau_p = 10.0$, 2dKA.

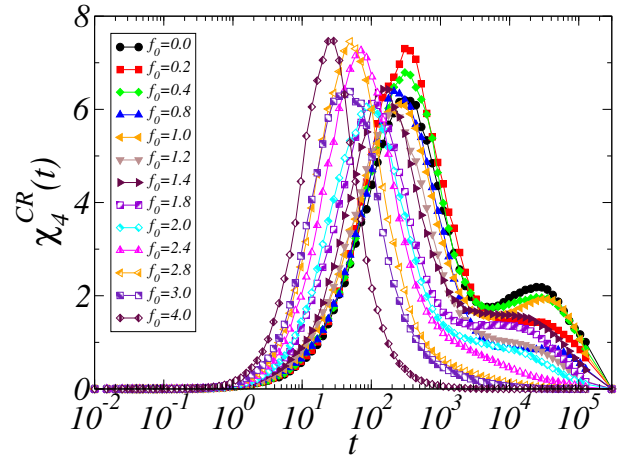


FIG. 4. ($\chi_4^{CR}(t)$ vs. t) for different f_0 of system size $N=50000$, at fixed $c=0.1$, $\tau_p = 10.0$ and $T=1.100$, 2dKA.

damped limits. We have set the system's diffusivity (D_0) to 1.0. As we know, the long-time behaviour of both Brownian dynamics (BD) and molecular dynamics (MD) is the same; we have kept all the parameters in the BD simulation the same as in the case of the MD simula-

tion. Now, we have taken a single canonical ensemble of extensive system $N = 50000$. Then, we used the Block Analysis to get the grand canonical ensemble average of the dynamical susceptibility ($\chi_4(t)$). We have taken a subsystem of size $L_B = L/3$, giving us 8 subsystems for

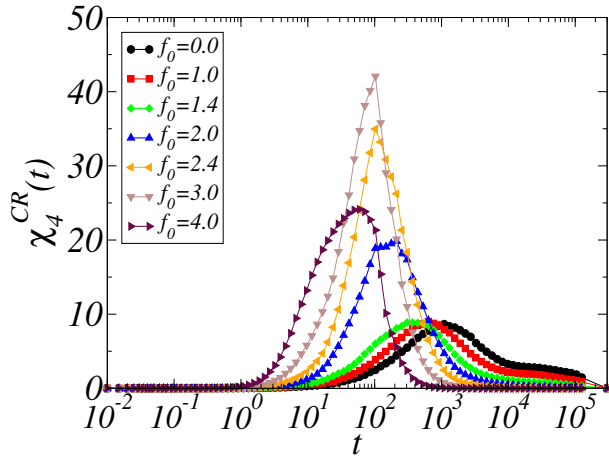


FIG. 5. ($\chi_4^{CR}(t)$ vs. t) for different f_0 of system size $N=50000$, at fixed $c=0.1$, $\tau_p = 100.0$ and $T=1.000$, 2dKA.

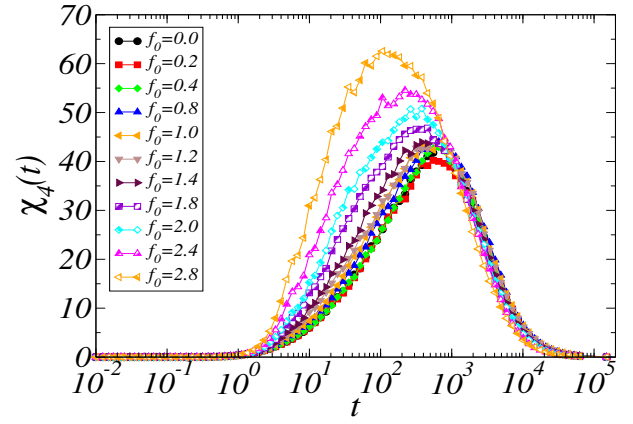


FIG. 7. $\chi_4(t)$ vs. t for different f_0 of system size $N = 50000$, $n_B = 3$ at fixed $c = 0.1$, $\tau_p = 10.0$, using Brownian dynamic simulation, 2dKA.

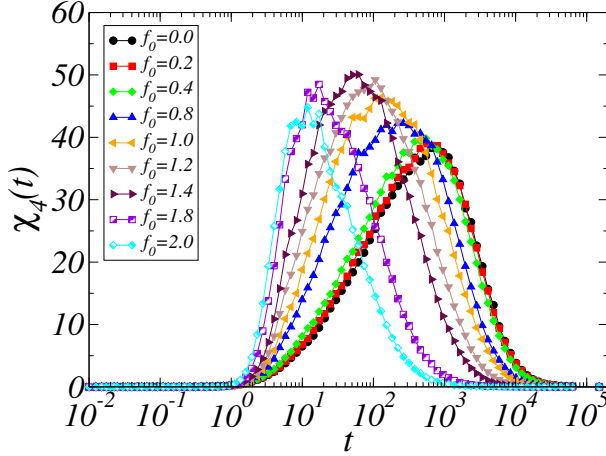


FIG. 6. $\chi_4(t)$ vs. t for different f_0 of system size $N = 50000$, $n_B=3$ at fixed $c = 0.1$, $\tau_p = 10.0$, using Brownian dynamic simulation, 2dmKA.

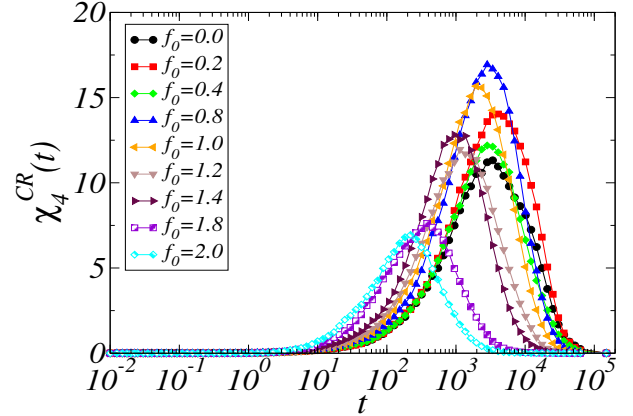


FIG. 8. ($\chi_4^{CR}(t)$ vs. t) for different f_0 of system size $N=50000$, at fixed $c=0.1$, $\tau_p = 10.0$, using Brownian dynamic simulation, 2dmKA.

averaging. As BD is in the over-damped limit here, the elastic long-wavelength mode should be suppressed considerably, and it should not mask the χ_4 peak around τ_α like MD simulation. In Fig. 6 χ_4^P fluctuates around 40 with changing activity in 2dmKA system. From Fig. 7, we can observe that χ_4^P is increasing with increasing activity from $f_0 = 1.8$. Again, we have measured the cage-relative $\chi_4(t)$ to neglect any possible collective motion in the system. In Fig. 8 for 2dmKA $\chi_4^{P,CR}$ tends to go down at higher activity, but In Fig. 9 we can observe the $\chi_4^{P,CR}$ to increase for different activity for 2dKA, unlike the normal glass (2dmKA). This analysis has been done on a single ensemble of $N = 50000$ system size; here also one observes the long time peak in Fig. 9 for 2dKA, now to understand this effect one needs further studies.

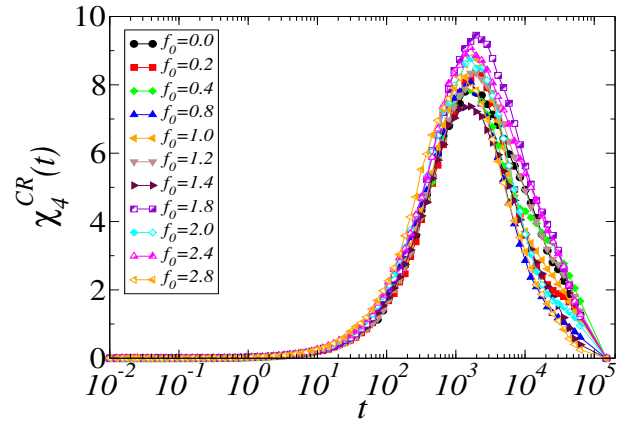


FIG. 9. ($\chi_4^{CR}(t)$ vs. t) for different f_0 of system size $N=50000$, at fixed $c=0.1$, $\tau_p = 10.0$, using Brownian dynamic simulation, 2dKA.

XI. MEAN SQUARE DISPLACEMENT FROM THE DYNAMICAL MATRIX

Taking the following Hamiltonian to describe the system

$$\mathcal{H} = \sum_{i=1}^N \frac{\vec{p}_i^2}{2m_i} + \frac{1}{2} \sum_{i \neq j} U(\vec{r}_i, \vec{r}_j), \quad (12)$$

if we assume that the harmonic approximation will be valid at low temperatures; position of the particles around an inherent structure(IS) can be written as:

$$\vec{r}_i = \vec{r}_{i,0} + \vec{u}_i \quad (13)$$

where, \vec{r}_i , $\vec{r}_{i,0}$ and \vec{u}_i represents the molecular dynamics trajectory, IS trajectory and small displacement from IS, respectively.

The Hamiltonian can be rewritten as:

$$\mathcal{H} \simeq \sum_{i=1}^N \frac{\vec{p}_i^2}{2m_i} + \frac{1}{2} H_{ij}^{\alpha\beta} u_i^\alpha u_j^\beta + V(\{\vec{r}_{i,0}\}) \quad (14)$$

where, $V(\{\vec{r}_{i,0}\}) = \frac{1}{2} \sum_{i \neq j} U(\vec{r}_i, \vec{r}_j)$. Lets take $m_i = 1$. Now the equation of motion becomes:

$$\ddot{u}_i = - \sum_{j\beta} H_{ij}^{\alpha\beta} u_j^\beta \quad (15)$$

where, $H_{ij}^{\alpha\beta} u_j^\beta = \left[\frac{\partial^2 V}{\partial r_i^\alpha \partial r_j^\beta} \right]_0$

Redefining the variables, $\{u_i^\alpha\} \rightarrow \{q_a\}$ and $\{\dot{u}_i^\alpha\} \rightarrow \{\dot{q}_a\}$; where $i = 1, 2, \dots, N$, $\alpha = 1, 2$ and $a = 1, 2, \dots, 2N$. Here, $a = (i-1)d + \alpha$ where d is the dimension. So, $u_i^\alpha = q_a = q_{(i-1)d+\alpha}$. Now the Hamiltonian becomes,

$$\mathcal{H} = V_0 + \frac{1}{2} \sum_i \dot{q}_a^2 + \frac{1}{2} \sum_{a,b} H_{ab} q_a q_b \quad (16)$$

And the equation of motions transforms as,

$$\ddot{q}_a = - \sum_b H_{ab} q_b \quad (17)$$

Now by performing an orthogonal transformation on $\underline{\mathcal{H}}$ we get,

$$\begin{aligned} \underline{\xi} &= \underline{S} \cdot \underline{q} \\ \underline{S} \cdot \ddot{\underline{q}} &= -\underline{S} \cdot \underline{\mathcal{H}} \cdot \underline{S}^{-1} \cdot \underline{S} \cdot \underline{q} \end{aligned} \quad (18)$$

So that, $\underline{D} = \underline{S} \cdot \underline{\mathcal{H}} \cdot \underline{S}^{-1}$ is diagonal, $D_{ab} = \lambda_a \cdot \delta_{ab}$
To find \underline{S} and $\{\lambda_a\}$ diagonalize $\underline{\mathcal{H}}$, $i.e$

$$\sum_b \mathcal{H}_{ab} o_b^{(n)} = \lambda_n o_a^{(n)} \quad (19)$$

Define $S_{ab} = o_a^{(n)}$ is orthogonal. The equations of motion for normal modes,

$$\begin{aligned} \ddot{\underline{\eta}} &= -\underline{D} \cdot \underline{\eta} \\ \text{so, } \ddot{\underline{\eta}}_a &= -\lambda_a \cdot \underline{\eta}_a \end{aligned} \quad (20)$$

Solving the above equation we get,

$$\eta_a(t) = \eta_a(0) \cos(\omega_a t) + \dot{\eta}_a(0) \frac{\sin(\omega_a t)}{\omega_a} \quad (21)$$

Now,

$$\begin{aligned} \underline{\eta}(t) &= \underline{S} \cdot \underline{q}(t) \\ \underline{q}(t) &= \underline{S}^{-1} \cdot \underline{\eta}(t) \\ q_a(t) &= \sum_b (S^{-1})_{ab} \cdot \eta_b(t) \end{aligned} \quad (22)$$

or,

$$q_a(t) = \sum_b o_a^b \cdot \eta_b(t) \quad (23)$$

Then the actual molecular dynamics trajectories can be written as:

$$r_i^\alpha(t) = r_i^\alpha(0) + \sum_b o_{(i-1)d+\alpha}^{(b)} \left[\eta_b \cos(\omega_b t) + \dot{\eta}_b \frac{\sin(\omega_b t)}{\omega_b} \right] \quad (24)$$

In the above summation, zero modes are excluded.

Now we will calculate the mean squared displacement using the above formalism,

$$\begin{aligned} (r_i^\alpha(t) - r_i^\alpha(0))^2 &= \sum_{\alpha,a,b} o_{(i-1)d+\alpha}^{(a)} o_{(i-1)d+\alpha}^{(b)} [\eta_a \eta_b (\cos(\omega_a t) - 1) (\cos(\omega_b t) - 1) + \\ & 2\dot{\eta}_a \dot{\eta}_b \frac{\sin(\omega_a t)}{\omega_a} (\cos(\omega_b t) - 1) + \dot{\eta}_a \dot{\eta}_b \frac{\sin(\omega_a t)}{\omega_a} \frac{\sin(\omega_b t)}{\omega_b}] \end{aligned} \quad (25)$$

So, after taking time origin average and ensemble average it becomes:

$$\begin{aligned} \langle (r_i^\alpha(t) - r_i^\alpha(0))^2 \rangle &= \sum_{\alpha, a, b} o_{(i-1)d+\alpha}^{(a)} o_{(i-1)d+\alpha}^{(b)} [\langle \eta_a \eta_b \rangle (\cos(\omega_a t) - 1)(\cos(\omega_b t) - 1) + \\ & 2 \langle \dot{\eta}_a \dot{\eta}_b \rangle \frac{\sin(\omega_a t)}{\omega_a} (\cos(\omega_b t) - 1) + \langle \dot{\eta}_a \dot{\eta}_b \rangle \frac{\sin(\omega_a t)}{\omega_a} \frac{\sin(\omega_b t)}{\omega_b}] \end{aligned} \quad (26)$$

$\langle \eta_a \eta_b \rangle = 0$ for $a \neq b$ and for $a = b$

$$\langle \eta_a \eta_b \rangle = \langle \eta_a^2 \rangle = \frac{\int d\eta_a e^{-\frac{\omega_a^2 \eta_a^2}{2K_B T}} \eta_a^2}{\int d\eta_a e^{-\frac{\omega_a^2 \eta_a^2}{2K_B T}}} = \frac{K_B T}{\omega_a^2}$$

$$\langle (r_i^\alpha(t) - r_i^\alpha(0))^2 \rangle = \sum_{\alpha, a} \left(o_{(i-1)d+\alpha}^{(a)} \right)^2 \left[K_B T \frac{(\cos(\omega_a t) - 1)^2}{\omega_a^2} + K_B T \frac{\sin^2(\omega_a t)}{\omega_a^2} \right] \quad (27)$$

So, Mean square displacement

$$\langle \Delta r(t)^2 \rangle = \frac{K_B T}{N} \left[\sum'_{a, i} (\vec{P}_i^a)^2 \frac{\sin^2(\omega_a t/2)}{(\omega_a/2)^2} \right]. \quad (28)$$

Where a is for all degrees of freedom ($d \cdot N$), and i is for all particles in the system N . ω_a is the a^{th} eigen frequency and \vec{P}_i^a is the i^{th} eigen vector corresponding to ω_a . The prime summation denotes that it is for non-zero eigenmodes only.

XII. ANALYSIS PROTOCOL OF DYNAMICAL MATRIX

Using the trajectories of particles, we calculate the displacement correlation matrix C_{ij} , which captures both local and long-range correlations in the particle motion. C_{ij} is defined as:

$$C_{ij} = \langle (\vec{r}_i(t) - \langle \vec{r}_i \rangle) \cdot (\vec{r}_j(t) - \langle \vec{r}_j \rangle) \rangle \quad (29)$$

where $\langle \dots \rangle$ represents the time average.

The relationship between the dynamical matrix and the actual Hessian of the system is given by $C_{ij}^{\alpha\beta} = \frac{1}{T} (\mathcal{H}_{ij}^{\alpha\beta})^{-1}$. Over time, $C_{ij}^{\alpha\beta}$ is expected to converge to $\mathcal{H}_{ij}^{\alpha\beta}$ as $t \rightarrow \infty$. However, practical constraints arise due to the limited computational runs and frames available for matrix generation. The eigenvalue distribution of the actual Hessian typically exhibits only d zero eigenmodes, where d represents the system's dimension. If a few frames are used to compute $C_{ij}^{\alpha\beta}$, the resulting distribution may show more than d zero eigenmodes. Nevertheless, increasing the number of frames tends to reduce

Similarly, $\langle \dot{\eta}_a \dot{\eta}_b \rangle = 0$ and $\langle \dot{\eta}_a \dot{\eta}_b \rangle = K_B T \delta_{ab}$
Now,

this discrepancy. To validate this observation, we analyzed a passive system and computed its Hessian, which enabled us to derive the density of states (DoS). As we progressively increased the number of frames, the DoS obtained from the correlation matrix increasingly converged to that obtained from the Hessian.

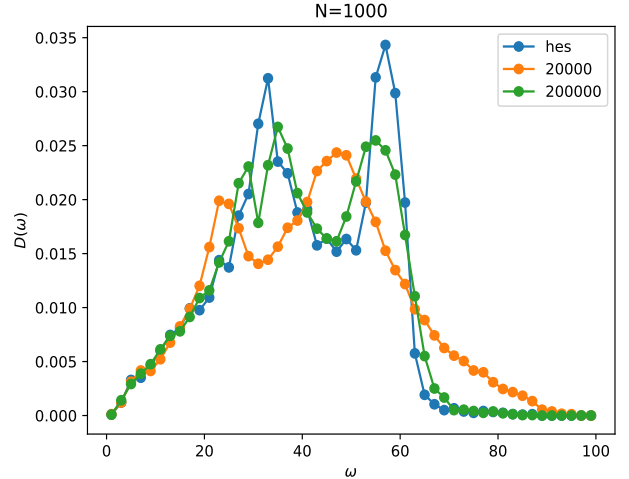


FIG. 10. $D(\omega)$ vs. ω for different number of frames from disp-disp correlation matrix compared with the DoS from hessian, poly-crystal system size $N = 1000$

However, the number of frames required for convergence depends entirely on the system size. As the system size increases, the necessary number of frames also increases rapidly. To quantify this, $R = N/T$ emerges as a crucial parameter, where T represents the number of independent time frames used for constructing the co-

variance matrix, and N denotes the number of degrees of freedom in the system. A $R < 1$ value ensures that the covariance matrix is constructed from independent measurements, while $R \rightarrow 0$ corresponds to the limit of perfect statistics. As R increases, the noise in the dynamical matrix also increases, leading to systematic errors in the density of states (DoS). Random matrix theory suggests that the eigenvalue distribution should converge linearly to its limiting values for disordered systems when $R = 0$.

Correction of DoS: As illustrated in Fig-11, eigenfrequencies ω_n exhibits a linear dependence on R . Thus, we analysed higher R values and extrapolated the data to $R \rightarrow 0$ to obtain the corrected eigenfrequencies. This correction significantly improved the convergence of the new DoS. A comparison between the corrected DoS and the DoS obtained from the Hessian is presented in the main text.

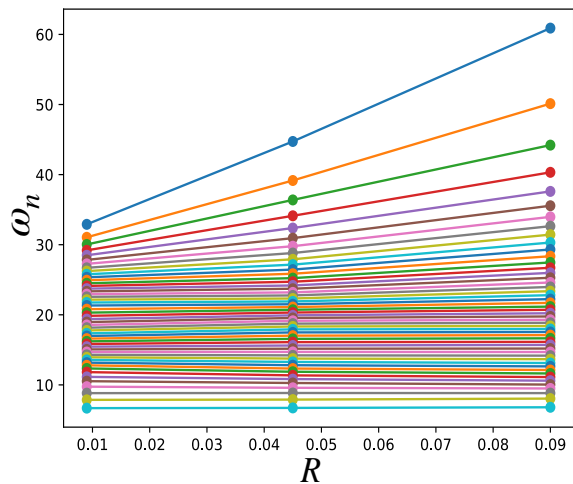


FIG. 11. eigen modes vs. R for system size $N = 1000$ poly-crystal

Force-force Correction Matrix: Similar to the displacement-displacement correlation matrix, we performed the same analysis for the force-force correlation matrix to get the DoS. $F_{ij}^{\alpha\beta}$ is defined as

$$F_{ij}^{\alpha\beta} = f_i^\alpha f_j^\beta \quad (30)$$

For the passive system, the convergence was pretty good (see Fig-13).

Using the eigenvectors and eigenvalues from the dynamical matrix, one can calculate the mean square displacement (MSD) via Eqn.28. We employed this approach to verify if the density of states (DoS) from the dynamical matrix provides accurate information about the system. We observed that the MSD from both force-force and displacement-displacement correlation matrices for passive systems matched the Molecular Dynamics MSD. However, for active systems, only the MSD from the displacement-displacement correlation matrix

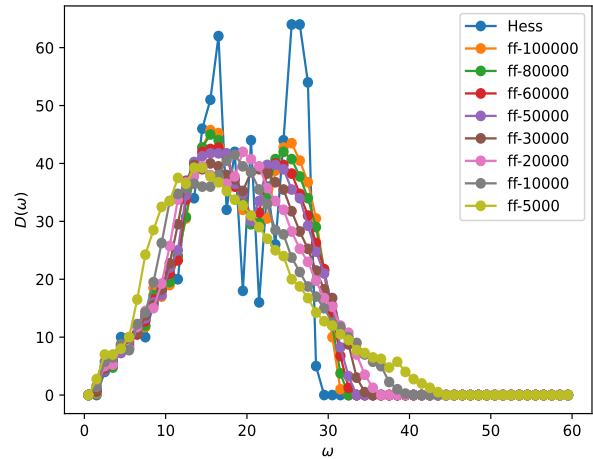


FIG. 12. $D(\omega)$ vs. ω for different numbers of frames from the ff-correlation matrix compared with the DoS from Hessian, system size $N = 400$ for crystal.

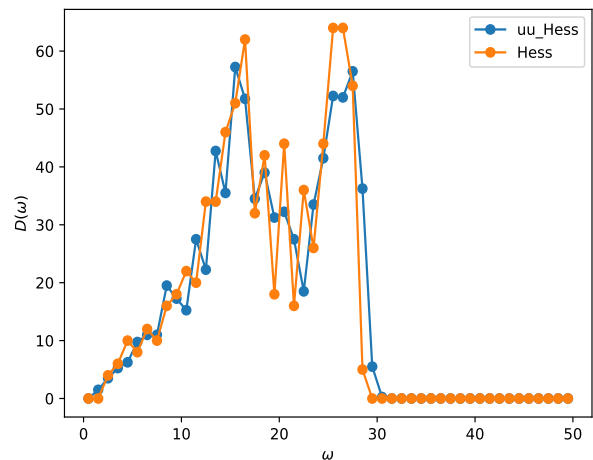


FIG. 13. Corrected DoS from ff-correlation matrix for system size $N = 400$ for crystal

showed good agreement (refer to the main text). In contrast, the force-force correlation MSD exhibited an opposite trend (refer to Fig-14). Therefore, for all further analyses, we utilized the displacement-displacement correlation.

Dispersion relation analysis: For each eigenmode obtained from the covariance matrix, the Fourier transform of its longitudinal and transverse components yields two spectral functions, denoted as f_L and f_T , respectively

$$f_T(q, \omega) = \left\langle \left| \sum_{j=1}^n \hat{\mathbf{q}} \times \mathbf{e}_{\omega, \mathbf{j}} e^{i\mathbf{q} \cdot \mathbf{r}_j} \right|^2 \right\rangle \quad (31)$$

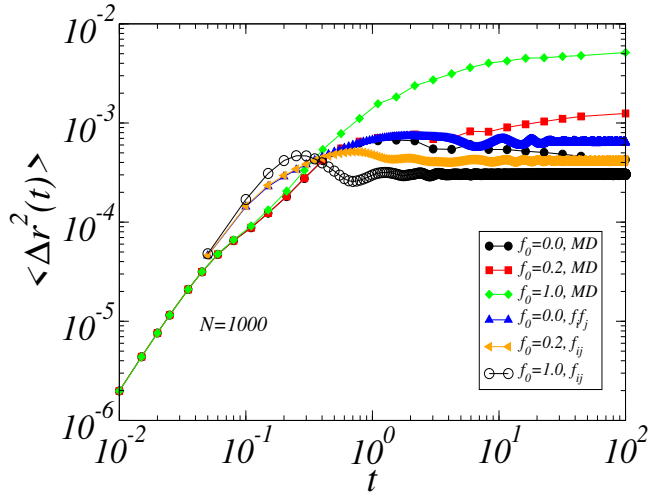


FIG. 14. MSD from molecular dynamics compared with MSD from ff-correlation matrix generated with 100000 frames, system size $N = 1000$

$$f_L(q, \omega) = \left\langle \left| \sum_{j=1}^n \hat{\mathbf{q}} \cdot \mathbf{e}_{\omega, j} e^{i\mathbf{q} \cdot \mathbf{r}_j} \right|^2 \right\rangle \quad (32)$$

where $\mathbf{e}_{\omega, j}$ is the polarization vector on the particle j in mode ω , \mathbf{q} is the wave vector.

Next, using the above formula, we binned f_L and f_T in the q - ω plane (refer to the heat map in the main text). Then, for each ω -bin, we fitted a Gaussian function in the vicinity of the peak of the f_L vs q and f_T vs q curves to obtain the corresponding q_{max} . This method allows us to determine the dispersion curve by extracting the peaks (refer to Fig 15-16).

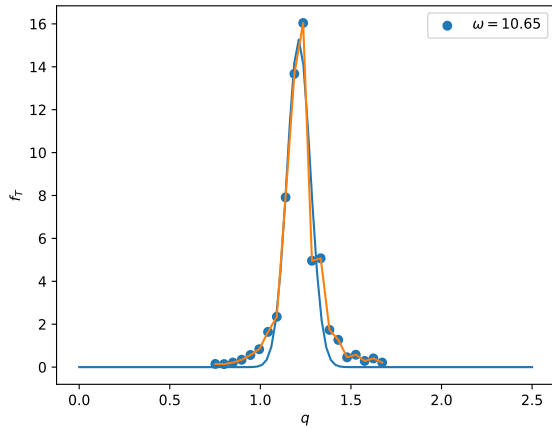


FIG. 15. f_T vs q for $\omega = 10.65$, $N = 4000$ poly-crystal and $f_0 = 1.0$. ($q_{max} = 1.21$)

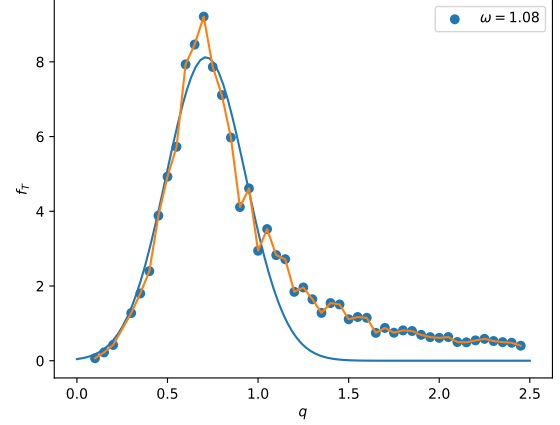


FIG. 16. f_T vs q for $\omega = 1.08$, $N = 4000$ glass and $f_0 = 1.0$. ($q_{max} = 0.712$)

XIII. DISPLACEMENT-DISPLACEMENT CORRELATION FUNCTION, $\Gamma(r, \Delta t)$

The dynamical length scale of the system ξ_d can be computed independently by computing the displacement-displacement correlation function $g^{uu}(r, t^*)$ at t^* [8, 9]. It is defined as,

$$g^{uu}(r, \Delta t) = \frac{\left\langle \sum_{i,j=1, j \neq i}^N u_i(0, \Delta t) u_j(0, \Delta t) \delta(r - |\mathbf{r}_{ij}(0)|) \right\rangle}{4\pi r^2 \Delta r N \rho \langle u(\Delta t) \rangle^2} \quad (33)$$

where, $u_i(t, \Delta t) = |\mathbf{r}_i(t + \Delta t) - \mathbf{r}_i(t)|$, and $\langle u^2(\Delta t) \rangle = \langle \frac{1}{N} \sum_{i=1}^N \mathbf{u}_i(t, \Delta t) \cdot \mathbf{u}_i(t, \Delta t) \rangle$. $g^{uu}(r, \Delta t)$ is calculated at time $\Delta t = t^*$, along with the usual pair correlation function $g(r)$ defined as,

$$g(r) = \frac{\left\langle \sum_{i,j=1, j \neq i}^N \delta(r - |\mathbf{r}_{ij}(0)|) \right\rangle}{4\pi r^2 \Delta r N \rho} \quad (34)$$

For far enough particles, the displacement over a large enough time duration would be decorrelated, and g^{uu} would equal $g(r)$. So the quantity $\Gamma(r, \Delta t) = g^{uu}(r, \Delta t)/g(r) - 1.0$ would decay to zero as a function of r . If one assumes the decay to be exponential, the area under the curve will provide us with the correlation length.

XIV. ORIENTATIONAL ORDER

Per particle hexatic order parameter:

$$\psi_6(\vec{r}_i, t) = \frac{1}{n_i} \sum_{j \in n_i}^N \exp(i6\theta_{ij}), \quad (35)$$

where n_i is the number of nearest neighbours of particles i . Hexatic correlation function:

$$g_6(r) = \frac{1}{\rho N} \left\langle \sum_{i \neq j} \psi_6(\vec{r}_i) \psi_6^*(\vec{r}_j) \delta(|\vec{r} - \vec{r}_j + \vec{r}_i|) \right\rangle \quad (36)$$

This Hexatic correlation function has been normalised using pair correlation function $g(r)$.

XV. DERIVATION OF THE DYNAMICAL MATRIX CALCULATION

Here we present the mathematical derivation of the inverse relation between the displacement-displacement covariant matrix \mathcal{C} with the Hessian matrix \mathcal{H} . We start

by writing the potential energy as

$$U = U_0 + \frac{1}{2} \langle u | \mathcal{H} | u \rangle + \mathcal{O}(u^3) + \dots \quad (37)$$

within Harmonic approximation keeping only up to squared displacements $|u\rangle$ in the expansion and \mathcal{H} is the hessian or the dynamical matrix of the system. If $|\psi_n\rangle$ is the eigenvector of the Hessian matrix, such that

$$\mathcal{H} |\psi_n\rangle = \lambda_n |\psi_n\rangle, \quad (38)$$

then we can write any vector using eigenvectors as basis set as $|u\rangle = \sum_n C_n |\psi_n\rangle$ and then rewrite the energy function as

$$U = U_0 + \frac{1}{2} \sum_{m,n} C_m C_n \langle \psi_m | \mathcal{H} | \psi_n \rangle = U_0 + \frac{1}{2} \sum_n C_n^2 \lambda_n, \quad (39)$$

where C_n are the amplitude of the n^{th} eigenvector on that given displacement vector $|u\rangle$. Given this, one can then compute the averaged displacement-displacement covariant matrix within Harmonic approximation (with $\mathcal{Z}_{\mathcal{N}}$ being the configurational partition function) as

$$\begin{aligned} \langle |u\rangle \langle u| \rangle &= \left\langle \sum_{m,n} C_m C_n |\psi_m\rangle \langle \psi_n| \right\rangle \propto \frac{1}{\mathcal{Z}_{\mathcal{N}}} \int \mathcal{D}C_p \exp(-\beta/2 \sum_p C_p^2 \lambda_p) \sum_{m,n} C_m C_n |\psi_m\rangle \langle \psi_n| \\ &= \sum_{m,n} \frac{|\psi_m\rangle \langle \psi_n|}{\mathcal{Z}_{\mathcal{N}}} \int \mathcal{D}C_p \exp(-\beta/2 \sum_p C_p^2 \lambda_p) C_m C_n \\ &= \sum_{m,n} |\psi_m\rangle \langle \psi_n| \left[\frac{\int dC_n \int dC_m \exp(-\beta/2(C_m^2 \lambda_m + C_n^2 \lambda_n)) \cdot C_n \cdot C_m}{\int dC_n \int dC_m \exp(-\beta/2(C_m^2 \lambda_m + C_n^2 \lambda_n))} \right] \\ &= \sum_{m,n} |\psi_m\rangle \langle \psi_n| \left[\frac{1}{\beta \lambda_n} \cdot \delta_{nm} \right] \\ &= k_B T \sum_{m,n} \frac{|\psi_m\rangle \langle \psi_n|}{\lambda_n} \\ &= k_B T \mathcal{H}^{-1}. \end{aligned}$$

Thus, we obtain the following relation between the displacement-displacement covariant matrix \mathcal{C} and the Hessian matrix \mathcal{H} as

$$\mathcal{C} = \langle |u\rangle \langle u| \rangle = k_B T \cdot \mathcal{H}^{-1}. \quad (40)$$

XVI. ADDITIONAL RELAXATION TIME DATA

In Fig. 17 shows the τ_{α}^{CR} as a function of temperature for both 2dmKA and 2dKA system. We used these data and the measured diffusion constant to next study the Stokes-Einstein breakdown in these systems. In Fig. 18,

we show the diffusivity D as a function of τ_{α} for all studied temperatures. We observe the breakdown of SE relation at high-temperature regime due to long-wavelength fluctuation in 2D system, which gets corrected once we remove the effect of long wavelength fluctuation via cage relative measurements or via Brownian dynamics simulations as in Fig. 19 with increasing damping D_0 the phonon modes get suppressed and one then recovers back the the usual Stokes-Einstein relation at high temperature, thereby proving that anomalous SE breakdown at high temperatures in these active liquids are also due to long wavelength phonon modes. In Fig. 20 it shows the relation of τ_{α} with cf_0^2 for both 2dmKA and

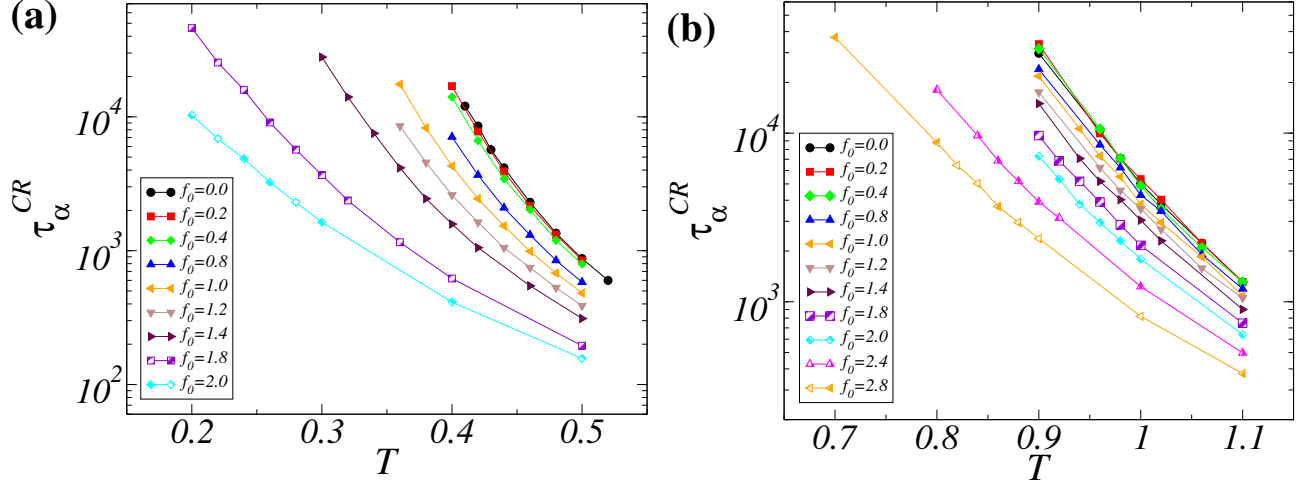


FIG. 17. (a) plot represents τ_α^{CR} vs T for different f_0 and fixed $c=0.1$ and $\tau_p = 1.0$, 2dmKA model (b) plots represents τ_α^{CR} vs T for different c and fixed $f_0 = 1.0$ and $\tau_p = 1.0$, 2dKA model.

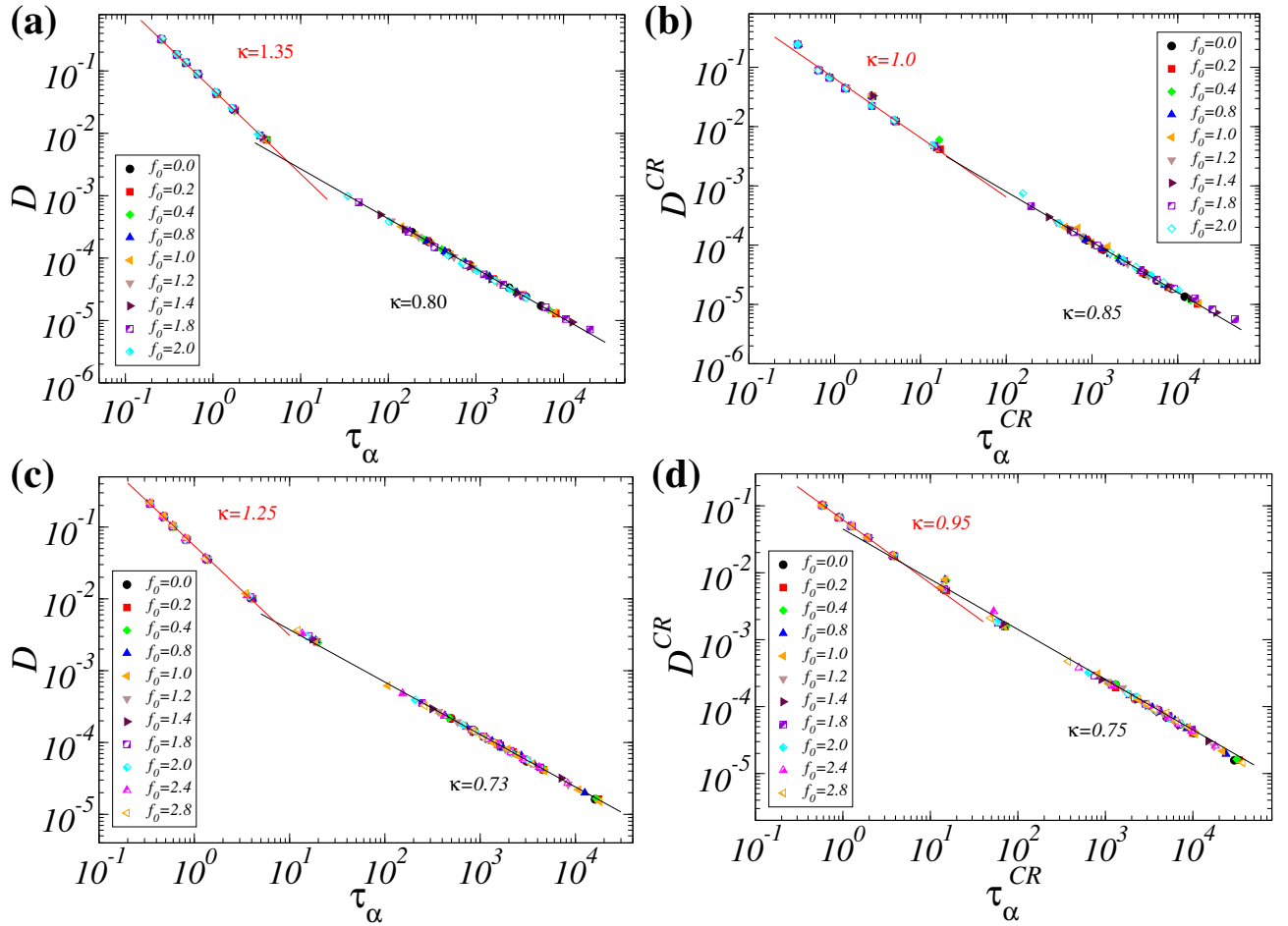


FIG. 18. D vs τ_α shows $D \propto \tau_\alpha^{-\kappa}$ in the supercooled regime for all active and passive system (a) & (b) for 2dmKA model, (c) & (d) for 2dKA model.

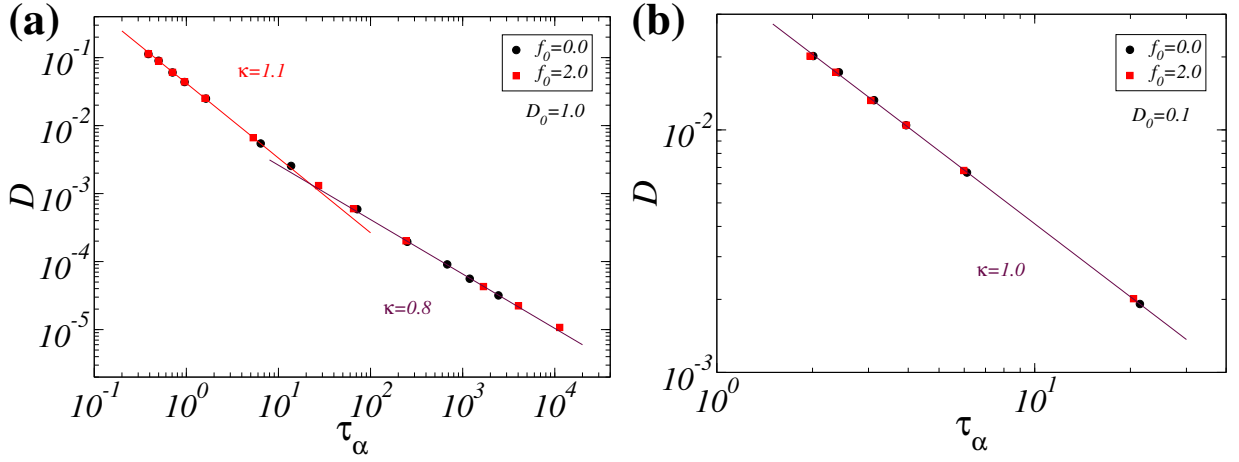


FIG. 19. D vs τ_α shows $D \propto \tau_\alpha^{-\kappa}$ in supercooled regime for all active and passive 2dmKA system with different damping (a) $D_0=1.0$ & (b) $D_0=0.1$.

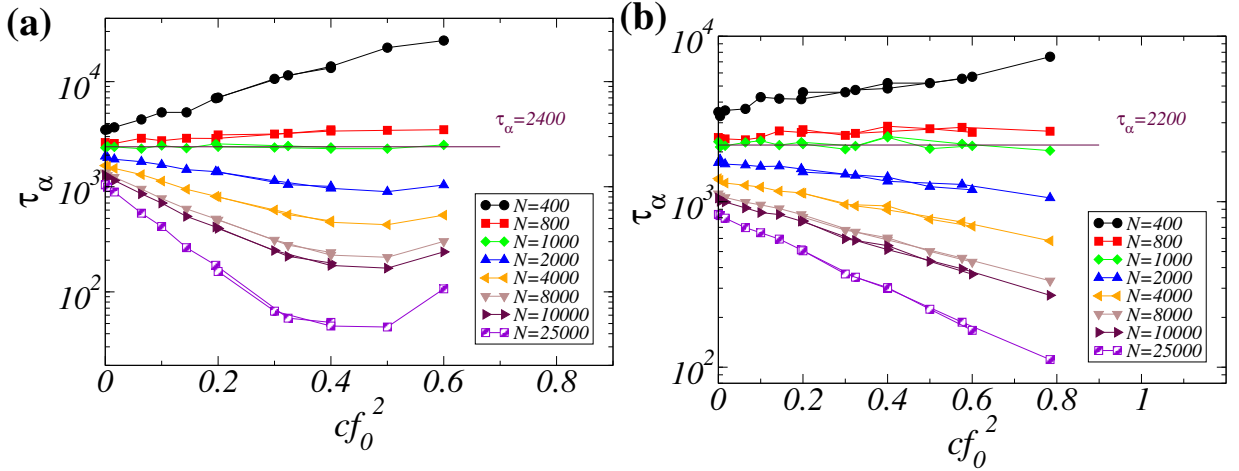


FIG. 20. (a) & (b) plots represents τ_α vs cf_0^2 . Here, both plots show the change in τ_α for different activity at their respective temperature, and the temperature is chosen such that τ_α for the $N=1000$ system remains. τ_α is set at 2400 for 2dmKA, and τ_α is set at 2200 for 2dKA. Temperature is kept the same for all the respective system sizes if not mentioned specifically. (a) plot is for the 2dmKA model, and (b) plot is for the 2dKA model.

2dKA. One striking observation of the 2dmKA is the non-monotonous nature of the τ_α with cf_0^2 , which is not present for the case of 2dKA in the present system.

XVII. ADDITIONAL ANALYSIS OF VDOs

In Fig. 21, we show the vibrational Density of States (VDoS) of 2dmKA model for all studied activities. A systematic increase in the weight of low frequency modes in the system with increasing activity is curiously similar to the VDoS observed in jamming to unjamming transition in soft sphere assemblies although in unjamming transition one does not get enhancement of phonon like modes in the system. We believe that enhancement of low frequency modes in active systems is primarily due to

coupling of active forces with the shear modes of the systems, although a detailed systematic analysis is needed to ascertain this angle of thought. We have a brief discussion on this aspect in the conclusion section of the main article. The right panel of the same figure shows the cumulative distribution function which seems to suggest that the initial power is close to 4 for passive system which then systematically changes to smaller power with increasing activity, although one needs much better statistics to reliably estimate the power law at small frequencies, so we do not want to discuss possible connections to quasi-localized modes and their power spectrum here.

In Fig., 22, a heat map of both the longitudinal mode and transverse mode is given for the 2dmKA model for a system size of $N = 4000$.

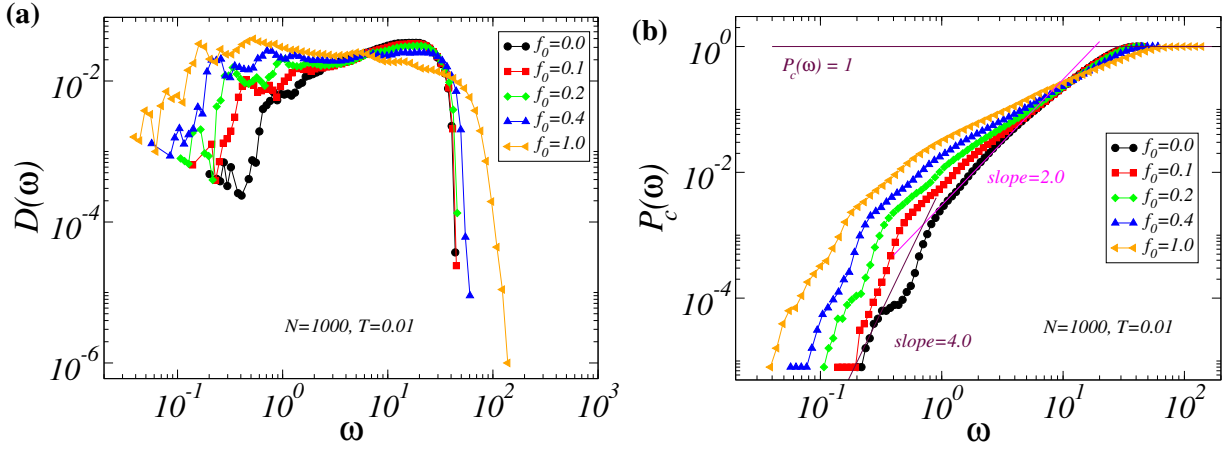


FIG. 21. (a) shows the Vibrational Density of States (VDoS) for the system size $N=1000$ for different activity, and (b) shows the cumulative density of states $P_c(\omega)$ for the the system size $N=1000$. Here, we have shown that the initial part of the effective VDoS increases rapidly with increasing activity.

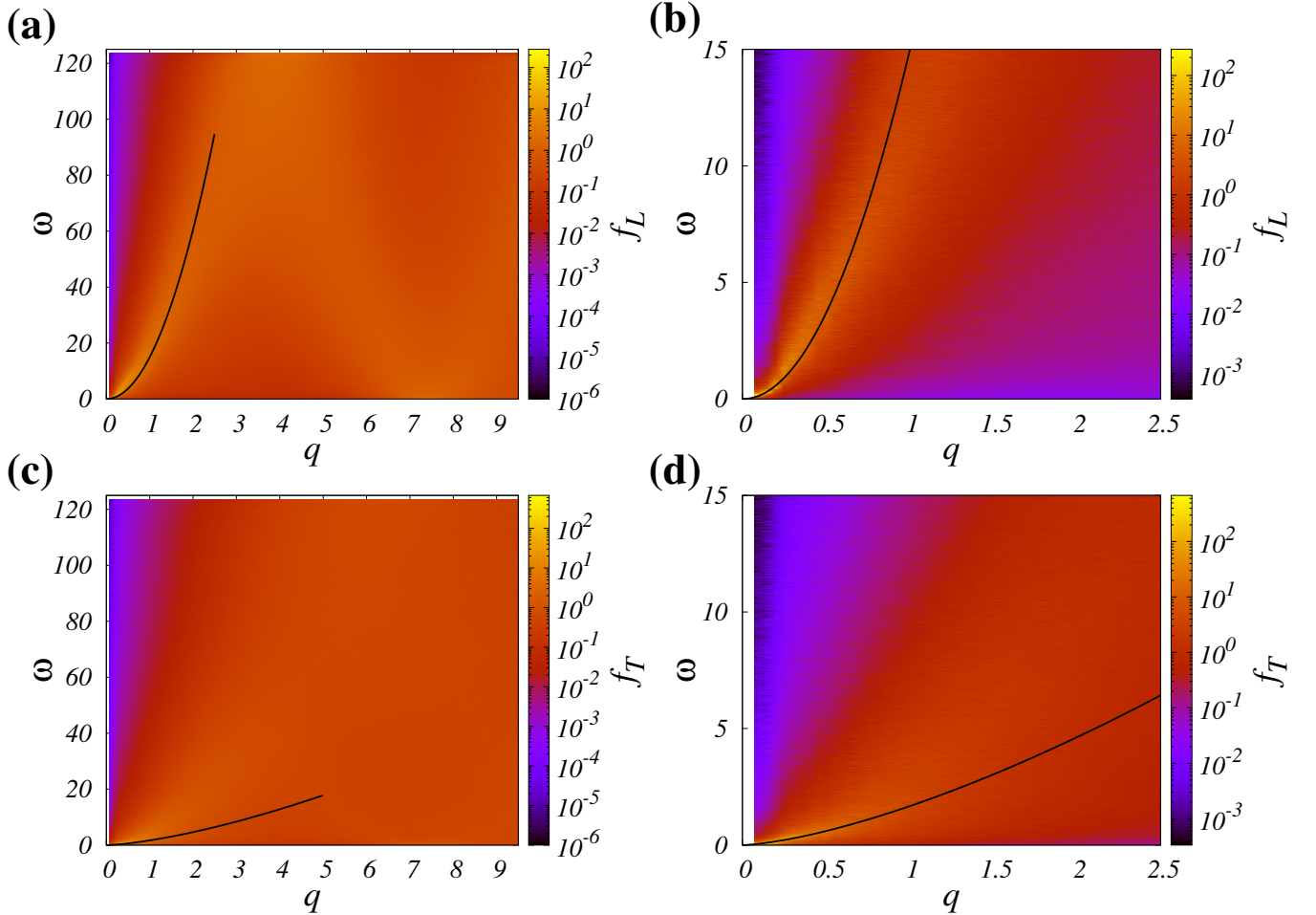


FIG. 22. Heat map: (a) & (b) are dispersion relations for longitudinal spectral function (f_L), (c) & (d) are dispersion relations for transverse spectral function (f_T). The system size $N=4000$ with activity $f_0 = 1.0$ shows deviation from the well-known linear phonon dispersion ($\omega \propto q$). For the active system, it clearly shows that the dispersion relation follows power-law behaviour ($\omega \propto q^\alpha$) in the small q regime, whereas for active system $\alpha > 1$ in both longitudinal and transverse spectrum. The power-law for f_L is $\omega \propto q^{2.02}$ and for f_T is $\omega \propto q^{1.47}$.

-
- [1] I. Tah, S. Sengupta, S. Sastry, C. Dasgupta, and S. Karmakar, *Phys. Rev. Lett.* **121**, 0850703 (2018).
 - [2] M. P. Allen and D. J. Tildesley, *Computer Simulation of Liquids* (Clarendon Press, New York, NY, USA, 1989).
 - [3] S. Mazoyer, F. Ebert, G. Maret, and P. Keim, *EPL (Europhysics Letters)* **88**, 66004 (2009).
 - [4] S. Vivek, C. P. Kelleher, P. M. Chaikin, and E. R. Weeks, *Proc. Nat. Acad. of Sci. (USA)* **114**, 1850 (2017).
 - [5] B. Illing, S. Fritschi, H. Kaiser, C. L. Klix, G. Maret, and P. Keim, *Proc. Nat. Acad. of Sci. (USA)* **114**, 1856 (2017).
 - [6] S. Chakrabarty, I. Tah, S. Karmakar, and C. Dasgupta, *Phys. Rev. Lett.* **119**, 205502 (2017).
 - [7] D. A. Beard and T. Schlick, *J. Chem. Phys.* **112**, 7313 (2000).
 - [8] I. Tah and S. Karmakar, *Phys. Rev. Research* **2**, 022067 (2020).
 - [9] P. H. Poole, C. Donati, and S. C. Glotzer, *Physica A: Statistical Mechanics and its Applications* **261**, 51 (1998).